Advances in Bioresearch
Adv. Biores., Vol 11 (6) November 2020: 248-273

Print ISSN 0976-4585; Online ISSN 2277-1573
Journal's URL:http://www.soeagra.com/abr.html
CODEN: ABRDC3
DOI: 10.15515/abr.0976-4585.11.6.248273

Advances in Bioresearch

ORIGINAL ARTICLE

In Silico Docking of EGFR and No Inhibitors as Anticancer Agents

[1]Umair Ahmed Nehal Ahmed*, [2]Shaikh Anwar Rafique, [3]Mohammed Ibrahim and [4]BakhshiAbdur Rahman Khalil Ahmed
[1,4]Jawaharlal Nehru Technological University, Kukatpally, Hyderabad, E-mail:
[2]Department of Pharmaceutical Chemistry, M.C.E. Society's, Allana College of Pharmacy, Azam Campus, Camp, Pune, Mahrashtra State-411 001
[3]Pratap Narender Reddy College of Pharmacy, Shamshabad(Man), Telangana – 509325
* Address for Correspondence

ABSTRACT
The epidermal growth factor receptor (EGFR) is a member of the protein kinase family, which is a clinically validated target for NSCLC / Liver cancer treatment. A novel series of compounds as EGFR and NO inhibitors were designed and evaluated for epidermal growth factor receptor inhibitory potential by using various computational tools along with NOS enzyme based cell line studies towards anti-cancer activity. Our docking studies evidenced that all the eight investigated compounds in comparison to reference molecule have the potential to dock inside the active binding pocket of the EGFR kinase domain with a binding energy in a range of -7.4 to -8.0 KJ /mol. The ligand LG6 has the lowest binding energy i.e. -8 kJ/mol among all eight compounds For NOS enzyme, the binding energy of reference molecule i.e. LG0 is -6.5 kJ/mol. The compound LG2 and LG4 have lowest binding energy among all docked compounds. LG 6 and LG 4 are having very low doc score/binding energies so both compounds were chosen for MD simulation studies. Molecular dynamic simulation studies for this compound LG 6 in complex with EGFR kinase domain has elucidated several interesting molecular level protein-ligand interactions with some of the important amino acid residues present at the active binding site of EGFR Kinase domain. convincingly, novel designed compound LG 6 of the present study have shown promising anti- cancer potential worth considering for further evaluations.
Keywords*: EGFR kinase, NOS Enzyme, Docking, Ligamd, MD simulations, Compounds, Anti-cancer.*

Received 10.10.2020 Revised 26.10.2020 Accepted 24.11.2020

How to cite this article:
U A N Ahmed, S A Rafique, M Ibrahim and B A R K Ahmed. *In Silico* Docking of EGFR and No Inhibitors as Anticancer Agent. Adv. Biores., Vol 11 (6) November 2020: 248-273

INTRODUCTION

Protein–ligand docking is a powerful tool to study and provide a proper understanding of protein–ligand interactions. Docking is regularly used in different stages of drug design strategies, such as to facilitate design of potentially active leads[1-2]. Detection of the best ligand poses and proper ranking of several ligands' relative docking propensity are of great importance. Molecular docking, in practice, has two essential requirements[3]: structural data, for candidate ligands and the protein target of interest, and a procedure to estimate protein–ligand interaction poses and strengths[4]. The RSCB Protein Data Bank (PDB) repository[5,6]is the main source of protein target structures for docking studies. The number of structures deposited in the PDB repository has been rapidly increasing for many years.

Cancer is one of the leading causes of mortality worldwide. Approximately one-third of people are affected by cancer during their lives[7]. In 2018, the American Cancer Society published the global cancer statistics 2018, which estimated that there will be about 18.1 million new cancer cases and 9.6 million cancer deaths worldwide[8].

The non-small cell lung cancer (NSCLC) represents the most prevalent lung cancer worldwide with less than 20% of 5-year survival rate after diagnosis[9].The epidermal growth factor receptor (EGFR) is a member of the protein kinase family, which is a clinically validated target for NSCLC treatment. EGFR is involved in various cellular signaling cascades, which are crucial in cell growth, proliferation, survival, and migration. Due to its crucial role, there have been continuous efforts to finda small molecule that is able to inhibit EGFR, particularly for the NSCLC treatment. Erlotinib and Gefitinib were considered as the

first-generation of EGFR inhibitors, which were used for the treatment of NSCLC[10]. However, it was known that the T790M point mutation in the EGFR, which was the substitution of Thr790 with Met residue had induced acquired resistance after a median of 10–14 months to most NSCLC patients of first-generation EGFR inhibitors[11]. Furthermore, Afatinib and Canertinib[12], two of several second-generation EGFR inhibitors, were approved by FDA for the treatment of metastatic NSCLC patients. However, the nonselective inhibition against wild type of EGFR has limitations in their clinical use[13].The third-generation EGFR inhibitors such as rociletinib and avitinib[14]. were developed; however, it was reported that the hyperglycemia was observed in NSCLC patients who used Rociletinib[15-17] designed and synthesized a series of phosphoramide mustard functionality, which was incorporated into the quinazoline scaffold, and their potential as EGFR inhibitors for the treatment of lung cancer was investigated. It was found that the designed compound could inhibit EGFR with IC50 at the nano molar range and showed no acute toxicity to mice at a single dose up to 900 mg/kg. It was concluded that the designed compound posed a potential as EGFR inhibitor. Based on these results, the present study was aimed to build a model of three-dimensional quantitative structure-activity relationship (3D-QSAR) including comparative molecular field analysis (CoMFA)[18] and comparative molecular similarity indices analysis (CoMSIA)[19]of quinazoline-phosphoramidate mustard conjugates. Using the built model, a novel compound was proposed, and molecular docking and molecular dynamics simulation were then used to check the conformational stability of the newly proposed compound in the binding site of EGFR.

Liver cancer is considered as one of the most widespread malignancies across the globe. According to a recent estimate, about 782,000 people were diagnosed for liver cancer, out of which 746,000 people died[20].Moreover, lung cancer accounts for about 5.6% of all new cancer cases diagnosed every year, and approximately 9.1% of all cancer related deaths across the globe[20]. The sharp increase in the incidence of liver cancer, lack of proper cure and the severe side-effects associated with the synthetic drugs has made it necessary to search for new and more effective molecules. In the past few decades, across the globe there has been a budding interest in the use of herbal drugs or herb-derived natural products, due to their lower side effects.Among the natural products, flavonoids form a large group of compounds ubiquitously found across plant kingdom[21]. These molecules have been reported to possess tremendous pharmacological properties, which include antimicrobial, antioxidant and anticancer activities[22]. The bioactivities of flavonoids are attributed to their ability to interact with a diversity of cellular enzymes. Moreover, flavonoids act as scavengers of reactive oxygen species (ROS), and also avert their formation by chelating metals[23, 24].

Macrophages are the main pro-inflammatory cells responsible for invading pathogens by releasing many pro-inflammatory molecules, including the free radical nitric oxide (NO) which is produced endogenously by the nitric oxide synthase (NOS) [25].Activated macrophages transcriptionally express inducible nitric oxide synthase (iNOS), which is responsible for the prolonged and profound production of NO. The aberrant release of NO can lead to amplification of inflammation as well as tissue injury [25].Therefore, inhibition of neutrophils and/or macrophages activation and the following release of inflammatory mediator NO provide a promising strategy for the development of potential anti-inflammatory agents. A number of synthetic and naturally occurring chalcone derivatives exhibit potent anti-inflammatory activities[26,27]. Although the mechanism of action is not yet fully understood. Anti-inflammatory activity of chalcones is associated with suppression of inflammatory mediators including NO [27]. Nitric oxide (NO) is an important molecule for host defense response against various pathogens such as bacteria, viruses, fungi, and parasites [28]. Under normal physiological conditions, NO plays an important role in the regulation of various pathophysiological processes such as neuronal Communication, vasodilatation, and neurotoxicity[29, 30]. However, overproduction of NO induces tissue damage associated with acute and chronic inflammations[31].Therefore, more attention is now being paid to the development of newdrugs as potent inhibitors of NO production in relation to the treatment of chronic inflammatory diseases[32].

NO is an intercellular mediator produced in various mammalian cells by three forms of Nitric oxide synthases (NOS) such as endothelium NO synthase (eNOS), neural NO synthase (nNOS) and inducible NO synthase (iNOS)[33]. Macrophages are important components of the mammalian immune system, and they play a key role by providing an immediate defence against foreign agents prior to leukocyte migration and production of various Pro-inflammatory mediators including the short-lived free radical NO[34].Lipopolysaccharide (LPS), a component from the cell walls of gram-negative bacteria and it is one of the most powerful activators of macrophages and involves the production of pro66 Inflammatory cytokines[35]. Therefore, inhibition of NO production in LPS67 Stimulated RAW 264.7 cells is one of the possible ways to screen various anti-inflammatory drugs.

MATERIAL AND METHODS

Table 1: Molecules in 2d and 3D format:

Compound	2-Dimensional structure	3-Dimensional structure (after minimization)
LG0 (Reference Molecule)	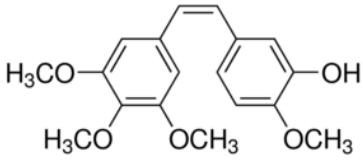	
LG1	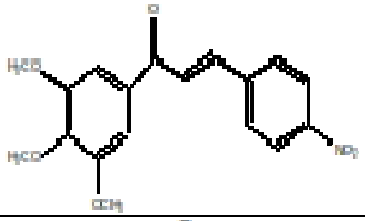	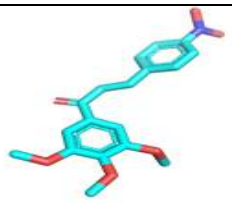
LG2	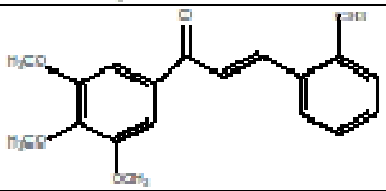	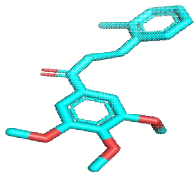
LG3	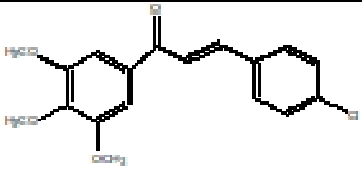	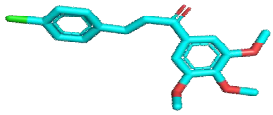
LG4	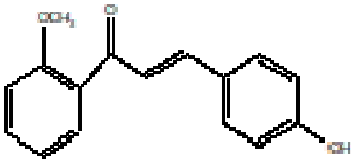	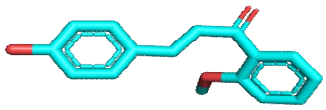
LG5	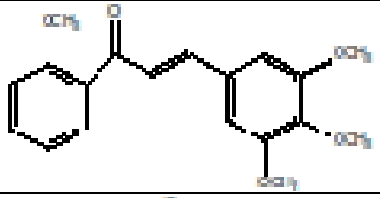	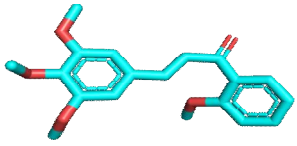
LG6	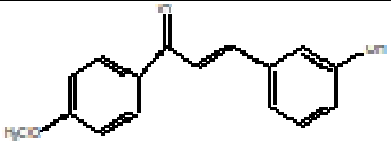	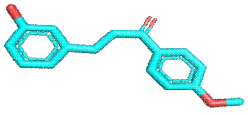
LG7	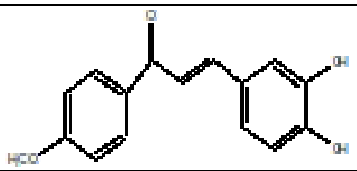	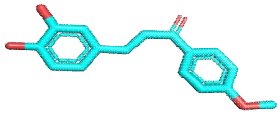
LG8	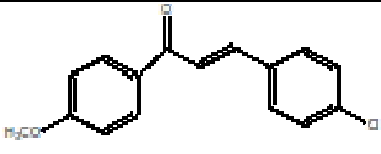	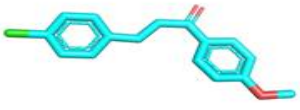

Receptor files with its image:

Fig.1 Epidermal Growth Factor Receptor(EGFR)

Fig.2 Nitric Oxide Synthase (NOS)

Docking chain (A or B or C):

Fig.3 Epidermal Growth Factor Receptor EGFR) Chain-A

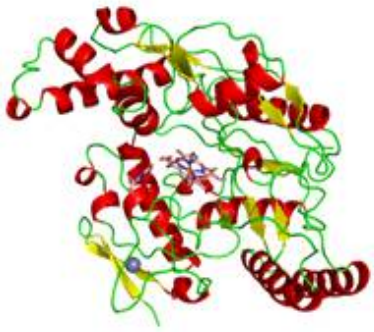

Fig.4 Nitric Oxide Synthase (NOS) Chain-C

Docking cavity images:

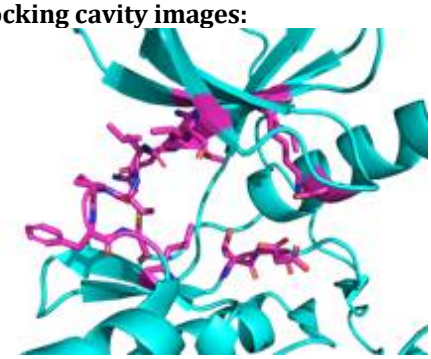

Fig.5 Epidermal Growth Factor Receptor (EGFR)

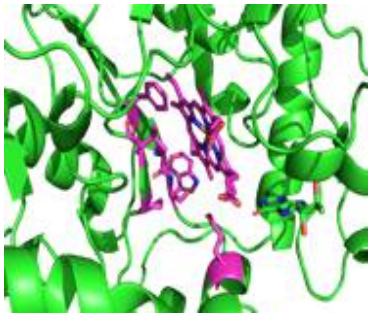

Fig.6 Nitric Oxide Synthase (NOS)

Docking methodology:

The EGFR and NOS enzyme receptor were used as docking target enzymes. The ligand structure was constructed using ChemDraw 2D. Then it was used to get three-dimensional structures of ligand using Chem3D. Also the ligand was energy minimized using MM2 force field present in Chem3D. Then, ligands and enzyme were prepared for docking using AutoDock Tools. The grid for docking was prepared using the inhibitor site and used it as a template. The Lamarkin GA was used to perform the docking. The docking was performed for 10 conformations and done used using AutoDock 4.2.6[36].The results were then analyzed using PyMOL and Chimera visualization software [37].

Receptor preparation:

The protein target structural file was selected from RCSB databank. The EGFR complex with inhibitor with PDB id 1M17 was used and for NOS, PDB id 4NOS was used for study. The EGFR PDB has only a chain. However, NOS pdb had 4 chains. It has been reported that NOS enzyme react in presence of Heme and HB4 compounds. Thus, the chain containing both compounds and Zinc ion which is present in chain C of pdb was extracted for study. The already bound inhibitors were removed and the resulting structures were used for minimization. The YASARA minimization server was used to minimize the structures. The Yasara viewer and PyMOL visualization server was used to visualize results.

Confirmer generation:
After docking the lowest energy structures were selected for each ligand and then they had been used for docking analysis.

RESULT AND DISCUSSION
Results with binding site, binding energies, binding interactions

Table2. Binding energy for EGFR enzyme:

Ligand	Binding energy(in kJ/mol)
LG0(Reference Molecule)	-7.4
LG1	-7.8
LG2	-7.7
LG3	-7.5
LG4	-7.9
LG5	-7.5
LG6	-8
LG7	-7.8
LG8	-7.6

Table3. Binding energy with NOS enzyme:

Ligand	Binding energy (in kJ/mol)
LG0 (Reference Molecule)	-6.5
LG1	-6.4
LG2	-7.2
LG3	-6.4
LG4	-7.2
LG5	-6.6
LG6	-6.8
LG7	-6.8
LG8	-6.6

Table-4 Interactions profile of EGFR with compounds

Reference Molecule LG0

Ligand	Ligand Atom	Chain	Residue	Residue number	Atom name	Chain	Distance(in Å)
LG0	O18	A	THR	766	OG1	A	3.26852
	O25	A	CYS	773	N	A	3.16328
	O40	A	ASP	831	N	A	3.38006
	O40	A	ASP	831	N	A	3.3898
	O40	A	THR	830	OG1	A	2.70397
LG1	O16	A	ASP	831	N	A	3.37184
	O16	A	ASP	831	N	A	3.38115
	O16	A	GLU	738	OE2	A	3.14549
	O26	A	MET	769	N	A	2.80648
	O16	A	THR	830	OG1	A	3.2
LG2	O7	A	ASP	831	OD2	A	3.35029
	O9	A	CYS	773	N	A	3.2267
LG3	O3	A	CYS	773	N	A	3.24285
	O6	A	MET	769	O	A	3.32925
	O6	A	MET	769	N	A	2.92111
LG4	O33	A	THR	830	OG1	A	3.2
	O30	A	MET	769	O	A	2.8
LG5	O44	A	THR	830	OG1	A	3.1
LG6	O2	A	THR	766	N	A	3.37218
	O2	A	THR	766	OG1	A	3.12643
	O2	A	LEU	764	O	A	2.72081
	O2	A	ALA	719	O	A	2.77804
	O2	A	LYS	721	N	A	3.4082
	O9	A	MET	769	O	A	3.26767
LG7	O27	A	LEU	764	O	A	3.05246
	O27	A	ALA	719	O	A	3.0899
	O27	A	THR	766	OG1	A	3.1
LG8	O24	A	MET	769	O	A	3.45226
	O24	A	MET	769	N	A	3.16788

Table-5 Interactions profile of NOS with compounds

Reference Molecule LG0

Ligand	Ligand Atom	Chain	Residue	Residue number	Atom name	Chain	Distance(in Å)
LG0	C7	A	GLU	377	OE1	C	3.43341
	C13	A	ASP	382	OD1	C	3.46548
	O18	A	TYR	373	OH	C	3.04258
	C30	A	GLN	263	OE1	C	3.49701
	O33	A	ALA	262	CB	C	3.46846
	O34	A	ARG	266	NH1	C	3.04586
	O40	A	TYR	347	OH	C	2.95439
	O40	A	ARG	266	NE	C	3.12165
LG1	C17	A	GLN	263	OE1	C	3.39937
	O26	A	ARG	266	NH1	C	3.04387
	O26	A	ARG	266	NH2	C	3.14895
	O27	A	VAL	352	CG2	C	3.28573
	O44	A	ASP	385	OD2	C	2.82209
	O44	A	ARG	381	NH1	C	2.80243
LG2	O16	A	GLU	377	OE1	C	3.44737
	C26	A	ASP	382	OD1	C	3.47553
LG3	O3	A	ARG	266	NH2	C	2.95481
	O13	A	ASP	385	OD2	C	3.21272
	C24	A	GLU	377	OE1	C	3.42893
	O32	A	ALA	282	CB	C	3.34621
LG4	O6	A	ARG	388	NH1	C	3.18483
	O6	A	ARG	388	NH2	C	3.32684
	O6	A	ASP	382	OD1	C	3.48639
	O6	A	ARG	266	NE	C	3.35414
	O6	A	ARG	266	NH2	C	3.01
	O30	A	ASN	354	ND2	C	2.98593
	O30	A	ASN	354	OD1	C	2.88653
LG5	C6	A	GLU	377	OE1	C	3.33451
	O10	A	ASN	354	OD1	C	3.30908
	O19	A	ASN	354	ND2	C	3.02218
	O24	A	ARG	266	NH2	C	3.03582
	O24	A	ARG	388	NH2	C	3.28133
	O24	A	ARG	388	NH1	C	3.1964
	O24	A	ARG	266	NE	C	3.3114
	O24	A	ASP	382	OD1	C	3.43492
	O44	A	ARG	388	NH2	C	3.2
LG6	O2	A	ARG	381	NH1	C	3.25058
	O2	A	ARG	381	NH2	C	2.89155
	O3	A	ARG	388	NH1	C	3.20278
	O3	A	ARG	388	NH2	C	3.24804
	O3	A	ARG	266	NE	C	3.32781
	O3	A	ASP	382	OD1	C	3.33223
	O3	A	ARG	266	NH2	C	3.13781
	O2	A	H4B	2011	C4	C	3
LG7	C22	A	GLN	263	OE1	C	3.45767
	O27	A	ARG	381	NH1	C	3.2751
	O27	A	ARG	381	NH2	C	2.95274
	O31	A	ARG	266	NH2	C	3.18497
	O31	A	ARG	388	NH2	C	3.29489
	O31	A	ARG	266	CZ	C	3.32189
	O31	A	ASP	382	OD1	C	3.34822
	O31	A	ARG	266	NE	C	3.29955
	O27	A	H4B	2011	O4	C	2.9
LG8	C20	A	GLN	263	OE1	C	3.47412
	O24	A	ARG	388	NH2	C	3.26649
	O24	A	ARG	266	NE	C	3.35882
	O24	A	ASP	382	OD1	C	3.32942
	O24	A	ARG	266	NH2	C	3.15539

Images of all interactions with residues:
Figures of EGFR docking:

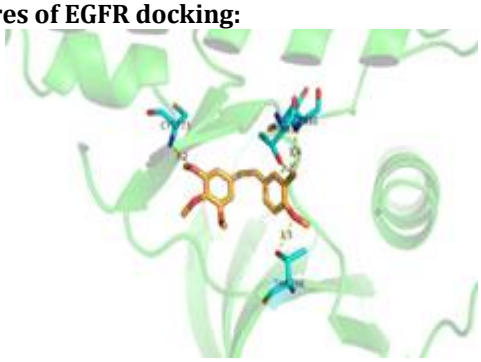

Fig.7 EGFR with compound LG0 (Reference Molecule)

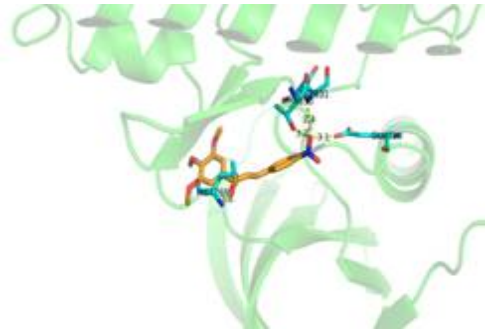

Fig.8 EGFR with compound LG1

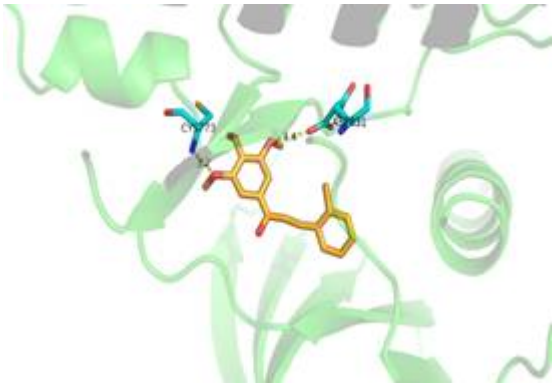

Fig.9 EGFR with compound LG2

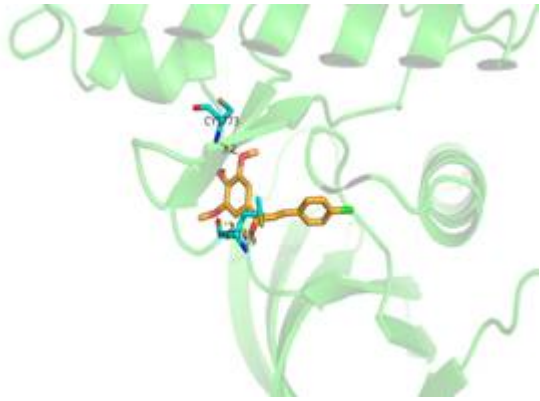

Fig.10 EGFR with compound LG3

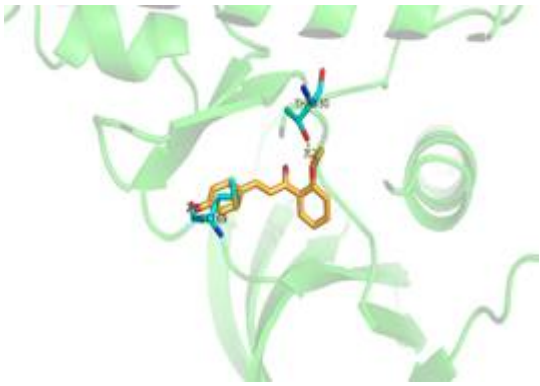

Fig.11 EGFR with compound LG4

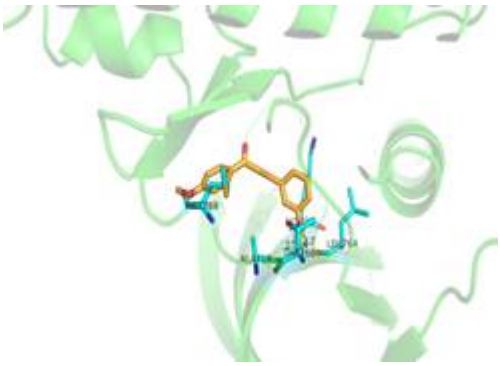

Fig.12 EGFR with compound LG5

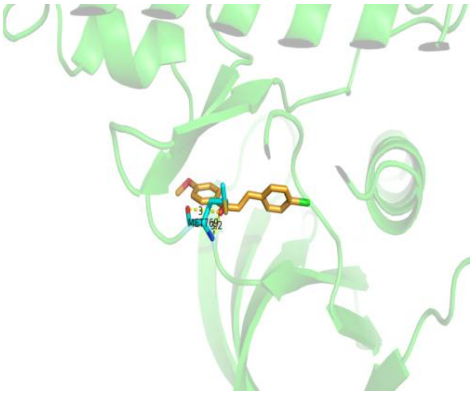

Fig.13 EGFR with compound LG6

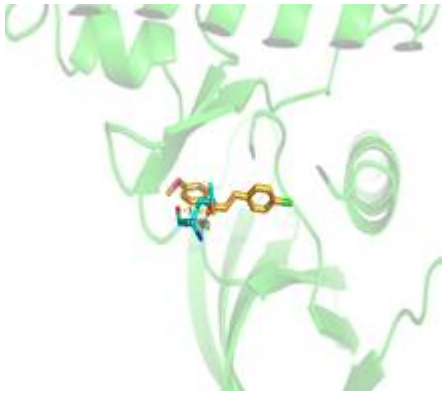

Fig.14 EGFR with compound LG7

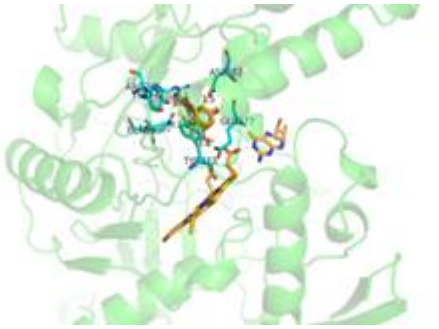

Fig.15 EGFR with compound LG8

Figures of NOS docking

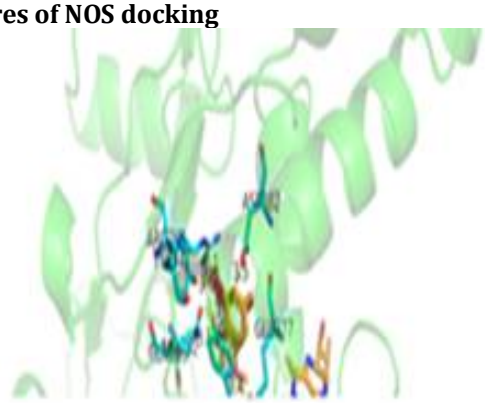

Fig.16 NOS with compound LG0 (Reference Molecule)

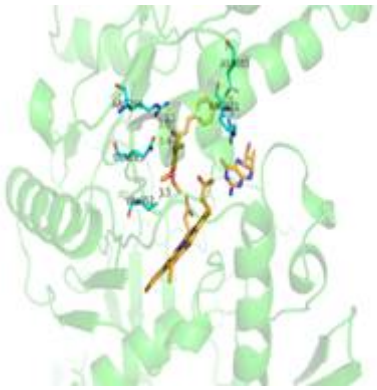

Fig.17 NOS with compound LG1

Fig.18 NOS with compound LG2

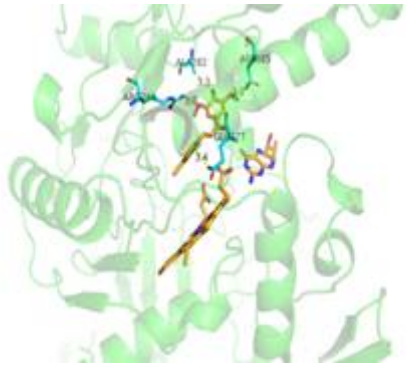

Fig.19 NOS with compound LG3

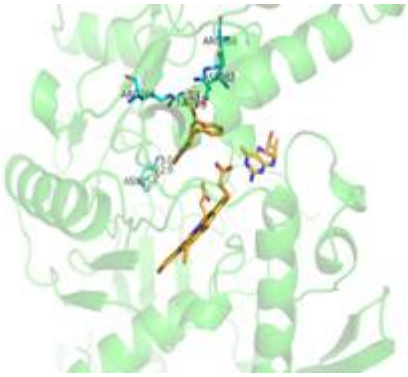

Fig.20 NOS with compound LG4

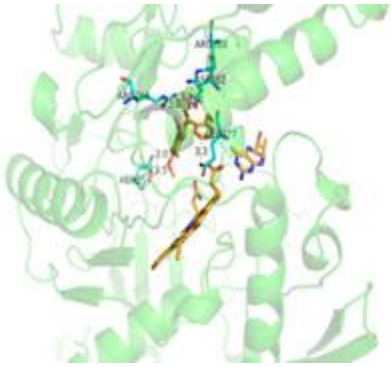

Fig.21 NOS with compound LG5

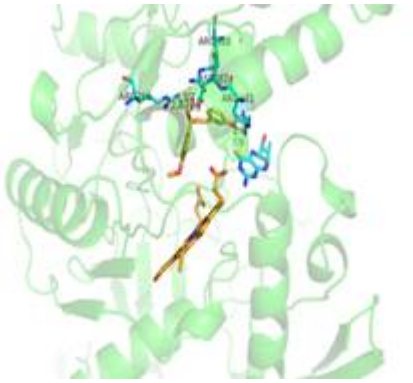

Fig.22 NOS with compound LG6

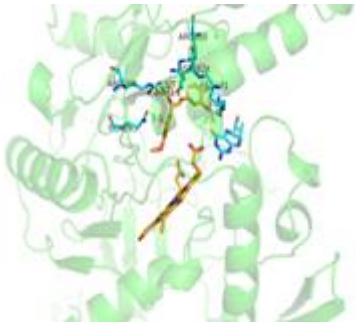

Fig.23 NOS with compound LG7

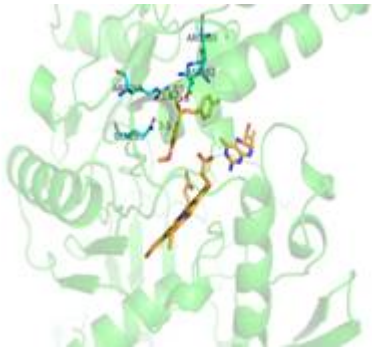

Fig.24 NOS with compound LG8

MD simulation of LG 4 and LG 6 because both are having very low doc score/binding energies so we have chosen both for MD simulation studies.

Simulation Interactions Diagram Report:

Simulation Details: Jobname: LG_04

Entry title: desmond_setup_26_3-out

CPU #	Job Type	Ensemble	Temp. [K]	Sim. Time [ns]	# Atoms	# Waters	Charge
1	Mdsim	NPT	300.0	40.042	45010	12675	0

Protein Information:

Tot. Residues	Prot. Chain(s)	Res. in Chain(s)	# Atoms	# Heavy Atoms	Charge
420	'C'	420	6749	3419	-2

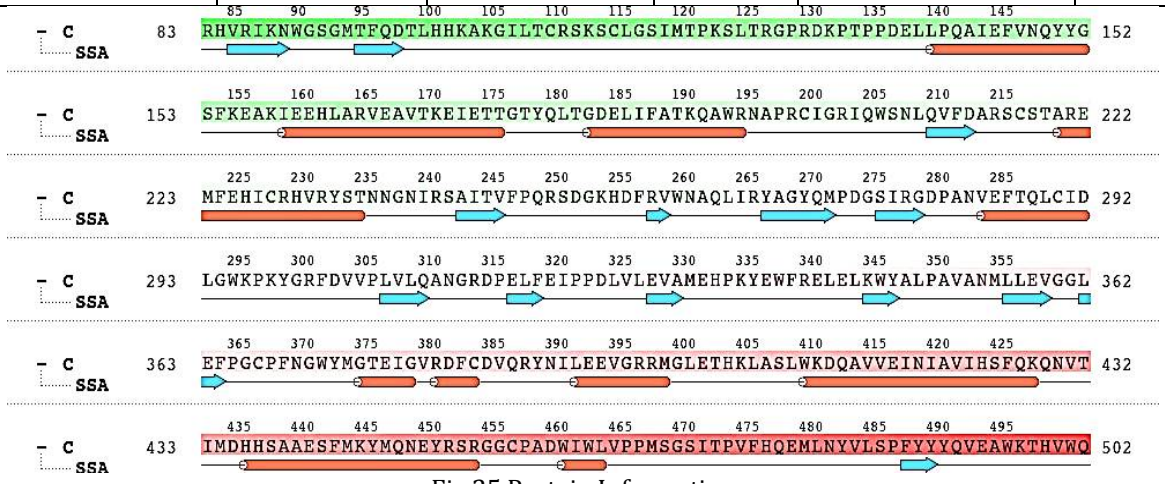

Fig.25 Protein Information

Ligand Information:

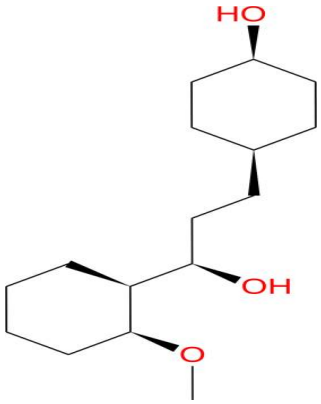

SMILE C1CCC[C@H](OC)[C@@H]1[C@H](O)CC[C@H]2CC[C@@H](O)CC2PDB Name 'LG4'

Num. of Atoms	49 (total) 19 (heavy)		
Atomic Mass	270.416 au		
Charge	0		
Mol. Formula	$C_{16}H_{30}O_3$	Num. of Fragments	1
Num. of Rot. Bonds	7		

Table 6: Counter Ion / Salt Information

Counter Ion /Salt Information:

Type	Number	Concentration (mM)	Total Charge
Zn	1	1.434	+2
Na	37	53.075	+37
Cl	35	50.206	-35

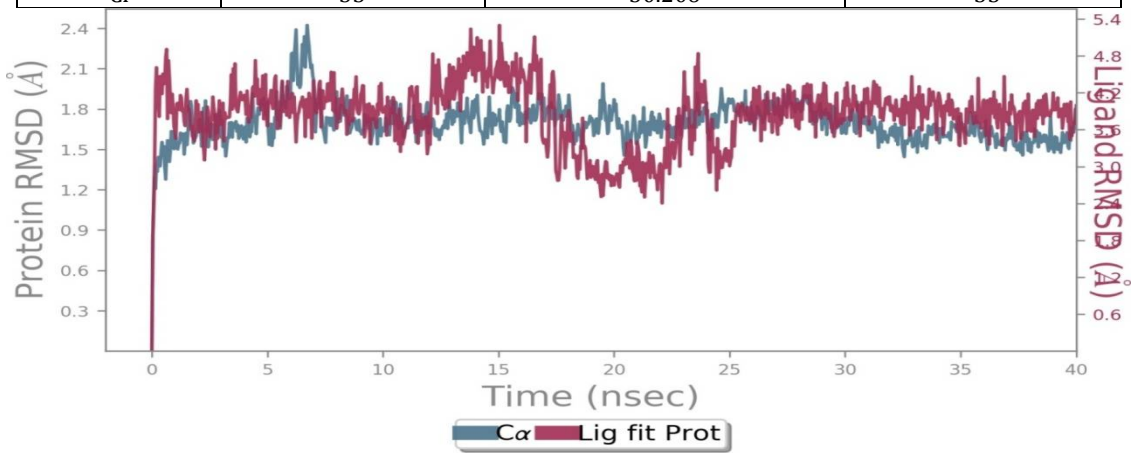

Fig.26 Protein-Ligand RMSD (Root Mean Square Deviation

Protein-Ligand RMSD. The Root Mean Square Deviation (RMSD) is used to measure the average change in displacement of a selection of atoms for a particular frame with respect to a reference frame. It is calculated for all frames in the trajectory. The RMSD for frame *x* is:

$$RMSD_x = \sqrt{\frac{1}{N}\sum_{i=1}^{N}(r_i'(t_x)) - r_i(t_{ref}))^2}$$

Where *N* is the number of atoms in the atom selection; t_{ref} is the reference time, (typically the first frame is used as the reference and it is regarded as time *t*=0); and *r'* is the position of the selected atoms in frame *x*after superimposing on the reference frame, where frame *x* is recorded at time t_x. The procedure is repeated for every frame in the simulation trajectory.

Protein RMSD: The above plot shows the RMSD evolution of a protein (left *Y*-axis). All protein frames are first aligned on the reference frame backbone, and then the RMSD is calculated based on the atom selection.

Monitoring the RMSD of the protein can give insights into its structural conformation throughout the simulation. RMSD analysis can indicate if the simulation has equilibrated - its fluctuations towards the

end of the simulation are around some thermal average structure. Changes of the order of 1-3 Å are perfectly acceptable for small, globular proteins. Changes much larger than that, however, indicate that the protein is undergoing a large conformational change during the simulation. It is also important that your simulation converges - the RMSD values stabilize around a fixed value. If the RMSD of the protein is still increasing or decreasing on average at the end of the simulation, then your system has not equilibrated, and your simulation may not be long enough for rigorous analysis.

Ligand RMSD:

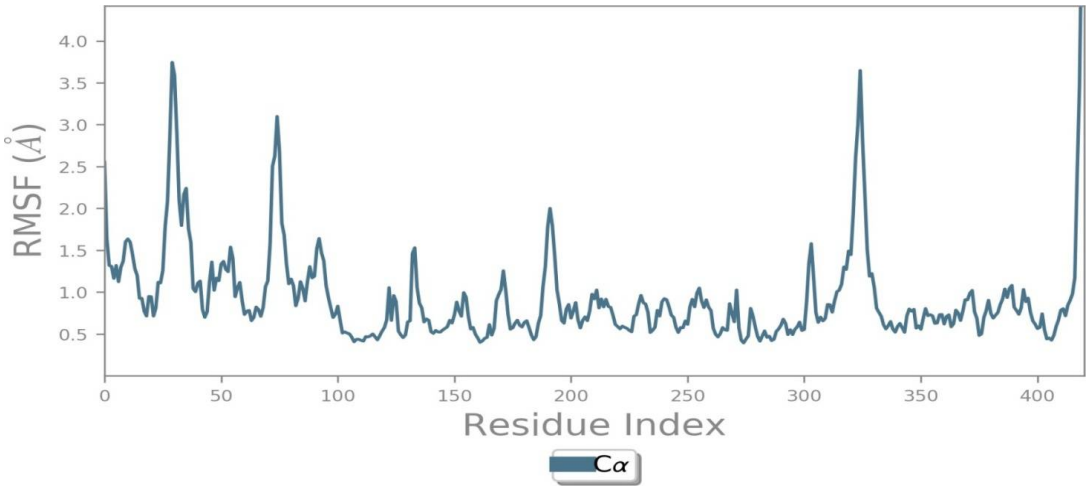

Fig.27 Protein RMSF (Root mean square Fluctuations)

Ligand RMSD (right *Y*-axis) indicates how stable the ligand is with respect to the protein and its binding pocket. In the above plot, 'Lig fit Prot' shows the RMSD of a ligand when the protein-ligand complex is first aligned on the protein backbone of the reference and then the RMSD of the ligand heavy atoms is measured. If the values observed are significantly larger than the RMSD of the protein, then it is likely that the ligand has diffused away from its initial binding site.

Protein RMSF

The Root Mean Square Fluctuation (RMSF) is useful for characterizing local changes along the protein chain. The RMSF for residue *i*is:

$$RMSF_i = \sqrt{\frac{1}{T}\sum_{t=1}^{T} < (r_i'(t)) - r_i(t_{ref}))^2 >}$$

where*T*is the trajectory time over which the RMSF is calculated, $t_{ref}$is the reference time, $r_l$is the position of residue *i*; *r'* is the position of atoms in residue *i*after superposition on the reference, and the angle brackets indicate that the average of the square distance is taken over the selection of atoms in the residue.

On this plot, peaks indicate areas of the protein that fluctuate the most during the simulation. Typically you will observe that the tails (*N*- and *C*-terminal) fluctuate more than any other part of the protein. Secondary structure elements like alpha helices and beta strands are usually more rigid than the unstructured part of the protein, and thus fluctuate less than the loop regions.

Protein Secondary Structure:

% Helix	% Strand	% Total SSE
27.02	12.25	39.27

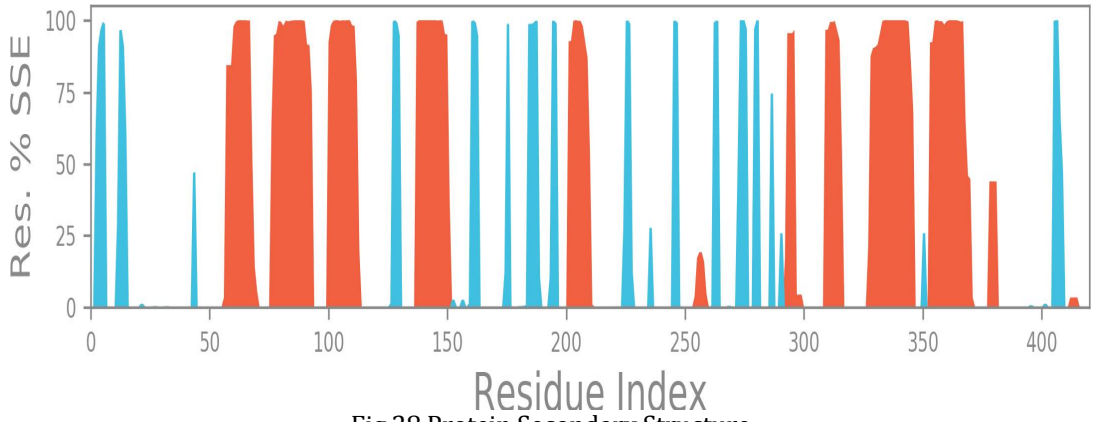

Fig.28 Protein Secondary Structure

Protein secondary structure elements (SSE) like alpha-helices and beta-strands are monitored throughout the simulation. The plot above reports SSE distribution by residue index throughout the protein structure. The plot below summarizes the SSE composition for each trajectory frame over the course of the simulation, and the plot at the bottom monitors each residue and its SSE assignment over time.

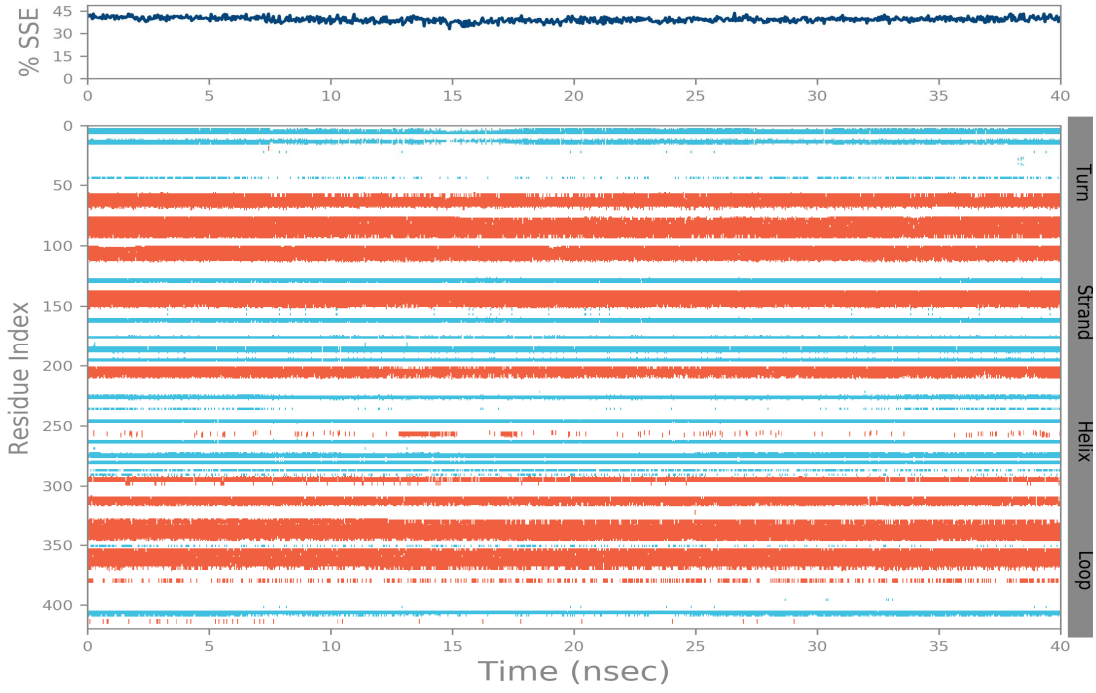

Fig.29 Protein Secondary Structure Elements

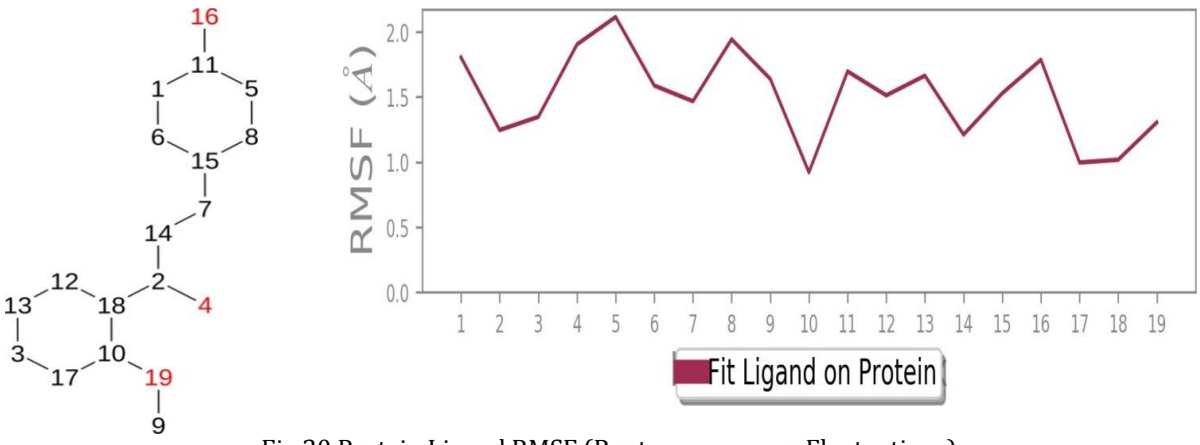

Fig.30 Protein Ligand RMSF (Root mean square Fluctuations)

Protein Ligand RMSF:

The Ligand Root Mean Square Fluctuation (L-RMSF) is useful for characterizing changes in the ligand atom positions. The RMSF for atom *i* is:

$$RMSF_i = \sqrt{\frac{1}{T}\sum_{t=1}^{T}(r_i'(t)) - r_i(t_{ref}))^2}$$

Where*T* is the trajectory time over which the RMSF is calculated, t_{ref} is the reference time (usually for the first frame, and is regarded as the *zero* of time); *r* is the position of atom *i*in the reference at time t_{ref} and *r'* is the position of atom *i*at time *t* after superposition on the reference frame.

Ligand RMSF shows the ligand's fluctuations broken down by atom, corresponding to the 2D structure in the top panel. The ligand RMSF may give you insights on how ligand fragments interact with the protein and their entropic role in the binding event. In the bottom panel, the 'Fit Ligand on Protein' line shows the ligand fluctuations, with respect to the protein. The protein-ligand complex is first aligned on the protein backbone and then the ligand RMSF is measured on the ligand heavy atoms.

Protein-Ligand Contacts:

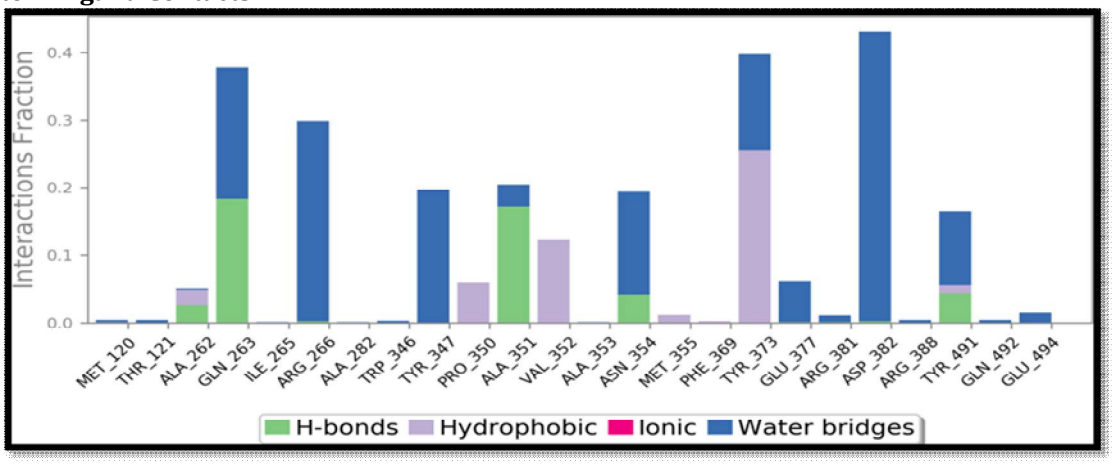

Fig. 31. Protein-Ligand Contacts

Protein interactions with the ligand can be monitored throughout the simulation. These interactions can be categorized by type and summarized, as shown in the plot above. Protein-ligand interactions (or 'contacts') are categorized into four types: Hydrogen Bonds, Hydrophobic, Ionic and Water Bridges. Each interaction type contains more specific subtypes, which can be explored through the 'Simulation Interactions Diagram' panel. The stacked bar charts are normalized over the course of the trajectory: for example, a value of 0.7 suggests that 70% of the simulation time the specific interaction is maintained.

Values over 1.0 are possible as some protein residue may make multiple contacts of same subtype with the ligand.

Hydrogen Bonds:

(H-bonds) play a significant role in ligand binding. Consideration of hydrogen-bonding properties in drug design is important because of their strong influence on drug specificity, metabolization and adsorption. Hydrogen bonds between a protein and a ligand can be further broken down into four subtypes: backbone acceptor; backbone donor; side-chain acceptor; side-chain donor.

The current geometric criteria for protein-ligand H-bond is: distance of 2.5 Å between the donor and acceptor atoms (D—H···A); a donor angle of 120° between the donor-hydrogen-acceptor atoms (D—H···A); and an acceptor angle of 90° between the hydrogen-acceptor-bonded atom atoms (H···A—X).

Hydrophobic contacts:

Falls into three subtypes: Cation; and Other, non-specific interactions. Generally these type of interactions involve a hydrophobic amino acid and an aromatic or aliphatic group on the ligand, but we have extended this category to also include Cation interactions.

The current geometric criteria for hydrophobic interactions is as follows:

Cation- Aromatic and charged groups within 4.5 Å; Two aromatic groups stacked face-to-face or face-to-edge; other; A non-specific hydrophobic sidechain within 3.6 Å of a ligand's aromatic or aliphatic carbons.

Ionic interactions: or polar interactions are between two oppositely charged atoms that are within 3.7 Å of each other and do not involve a hydrogen bond. We also monitor Protein-Metal-Ligand interactions, which are defined by a metal ion coordinated within 3.4 Å of protein's and ligand's heavy atoms (except carbon). All ionic interactions are broken down into two subtypes: those mediated by a protein backbone or side chains.

Water Bridges: are hydrogen-bonded protein-ligand interactions mediated by a water molecule. The hydrogen-bond geometry is slightly relaxed from the standard H-bond definition.

The current geometric criteria for a protein-water or water-ligand H-bond are: a distance of 2.8 Å between the donor and acceptor atoms (D—H···A); a donor angle of 110° between the donor-hydrogen-acceptor atoms (D—H···A); and an acceptor angle of 90° between the hydrogen-acceptor-bondedatom atoms (H···A—X).

Protein-Ligand Contacts (cont.)

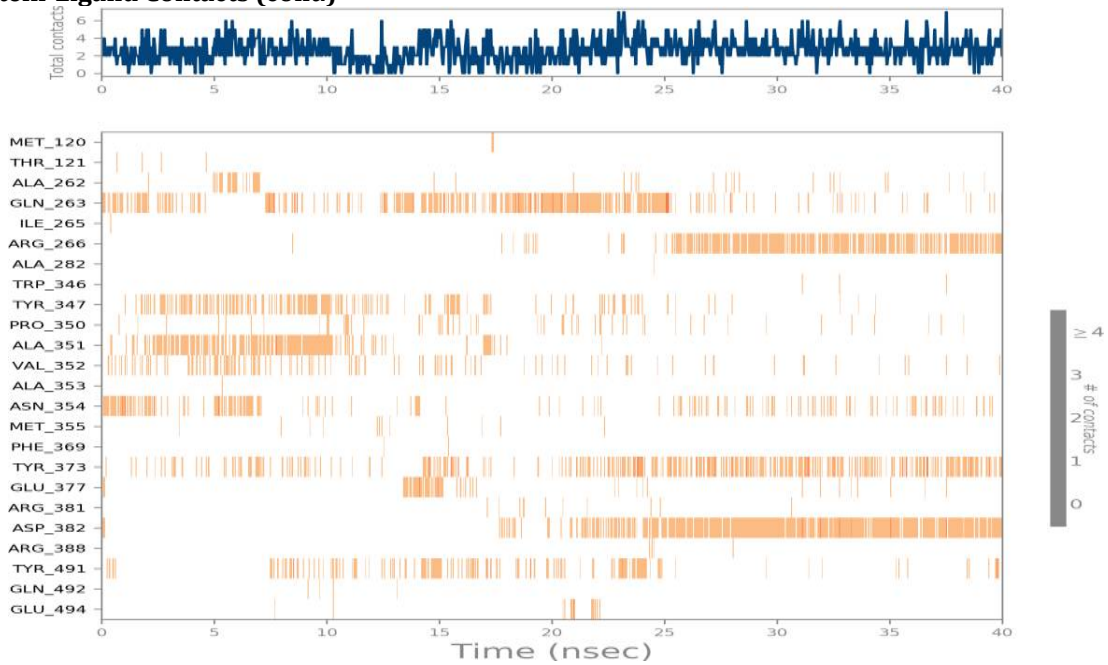

Fig.32.Protein-Ligand Contacts

A timeline representation of the interactions and contacts (**H-bonds**, **Hydrophobic**, **Ionic**, **Water bridges**) summarized in the previous page. The top panel shows the total number of specific contacts the protein makes with the ligand over the course of the trajectory. The bottom panel shows which residues interact with the ligand in each trajectory frame. Some residues make more than one specific contact with the ligand, which is represented by a darker shade of orange, according to the scale to the right of the plot.

Ligand-Protein Contacts:

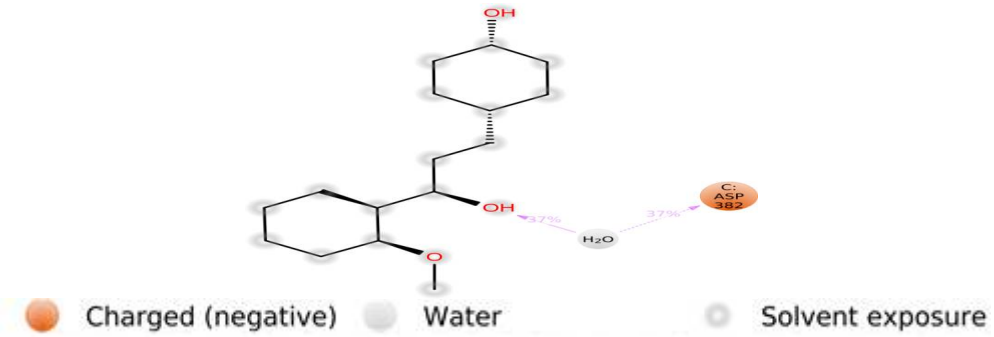

Fig.33.ligand atom interactions with the protein residues

A schematic of detailed ligand atom interactions with the protein residues. Interactions that occur more than **30.0%** of the simulation time in the selected trajectory (0.00 through 40.00 nsec), are shown.

Note: it is possible to have interactions with >100% as some residues may have multiple interactions of a single type with the same ligand atom. For example, the ARG side chain has four H-bond donors that can all hydrogen-bond to a single H-bond acceptor.

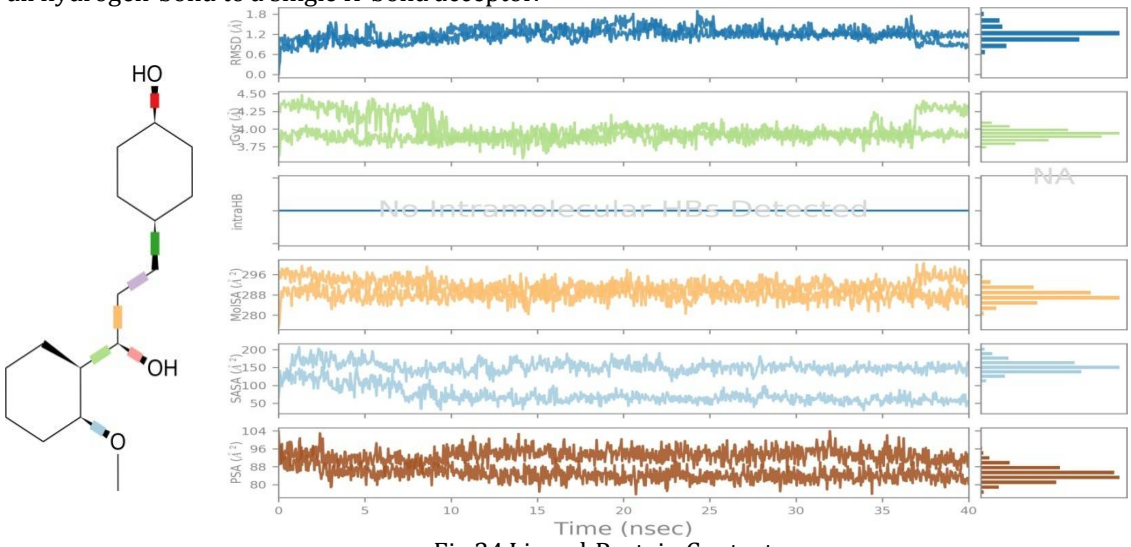

Fig.34.Ligand-Protein Contacts

Ligand Torsion Profile

The ligand torsions plot summarizes the conformational evolution of every rotatable bond (RB) in the ligand throughout the simulation trajectory (0.00 through 40.00 nsec). The top panel shows the 2d schematic of a ligand with color-coded rotatable bonds. Each rotatable bond torsion is accompanied by a dial plot and bar plots of the same color.

Dial (or radial) plots describe the conformation of the torsion throughout the course of the simulation. The beginning of the simulation is in the center of the radial plot and the time evolution is plotted radially outwards.

The bar plots summarize the data on the dial plots, by showing the probability density of the torsion. If torsional potential information is available, the plot also shows the potential of the rotatable bond (by summing the potential of the related torsions). The values of the potential are on the left *Y*-axis of the chart, and are expressed in *kcal/mol*. looking at the histogram and torsion potential relationships may give insights into the conformational strain the ligand undergoes to maintain a protein-bound conformation.

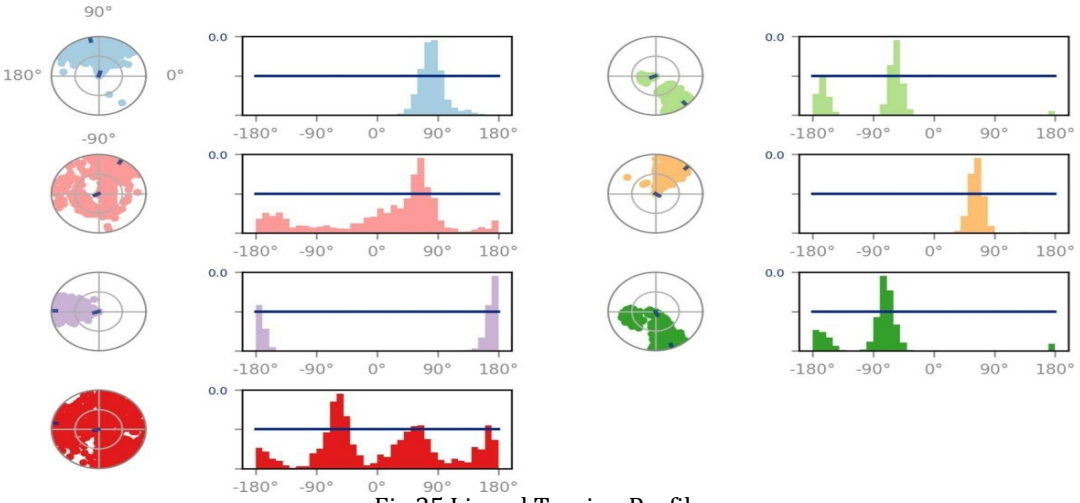

Fig.35.Ligand Torsion Profile

Ligand Properties

Ligand RMSD: Root mean square deviation of a ligand with respect to the reference conformation (typically the first frame is used as the reference and it is regarded as time *t*=0).

Radius of Gyration (rGyr): Measures the 'extendedness' of a ligand, and is equivalent to its principal moment of inertia.

Intramolecular Hydrogen Bonds (intraHB): Number of internal hydrogen bonds (HB) within a ligand molecule.

Molecular Surface Area (MolSA): Molecular surface calculation with 1.4 Å probe radius. This value is equivalent to a van der Waals surface area.

Solvent Accessible Surface Area (SASA): Surface area of a molecule accessible by a water molecule.

Polar Surface Area (PSA): Solvent accessible surface area in a molecule contributed only by oxygen and nitrogen atoms.

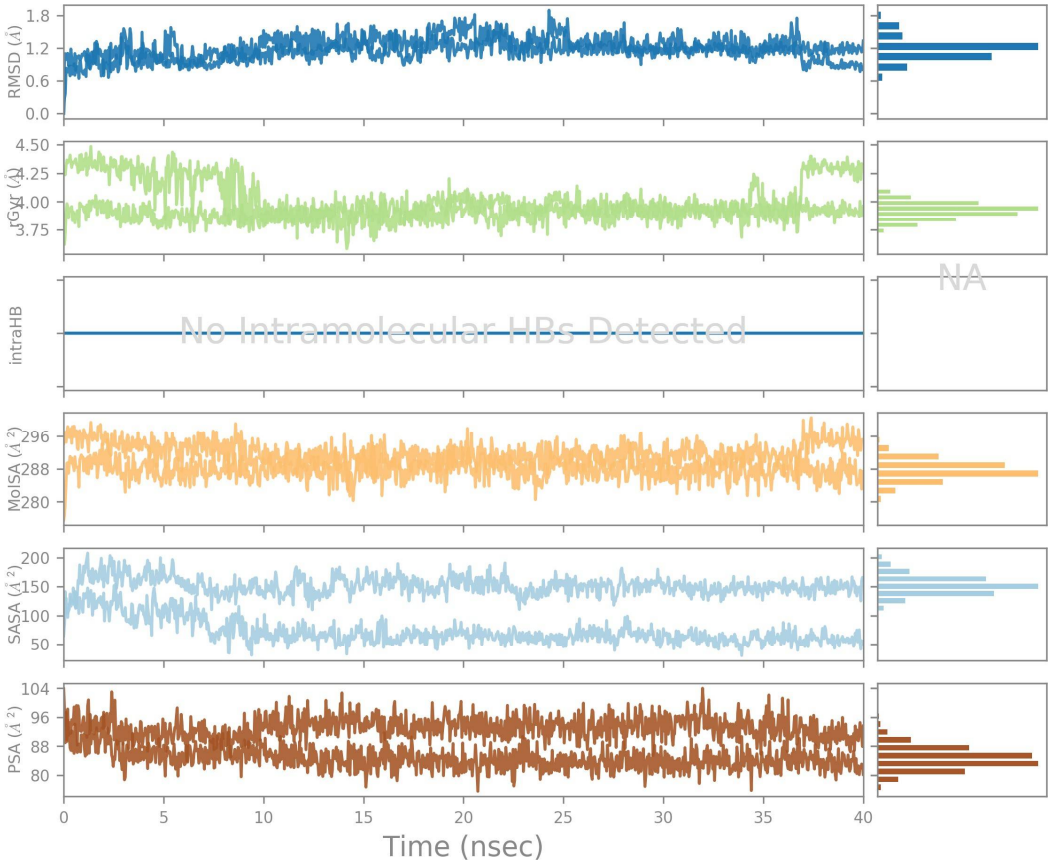

Fig.36.Ligand Properties

Simulation Interactions Diagram Report
Simulation Details
Jobname: LG_06
Entry title: AM_06_3-out

CPU #	Job Type	Ensemble	Temp. [K]	Sim. Time [ns]	# Atoms	# Waters	Charge
1	mdsim	NPT	300.0	40.042	55030	16617	0

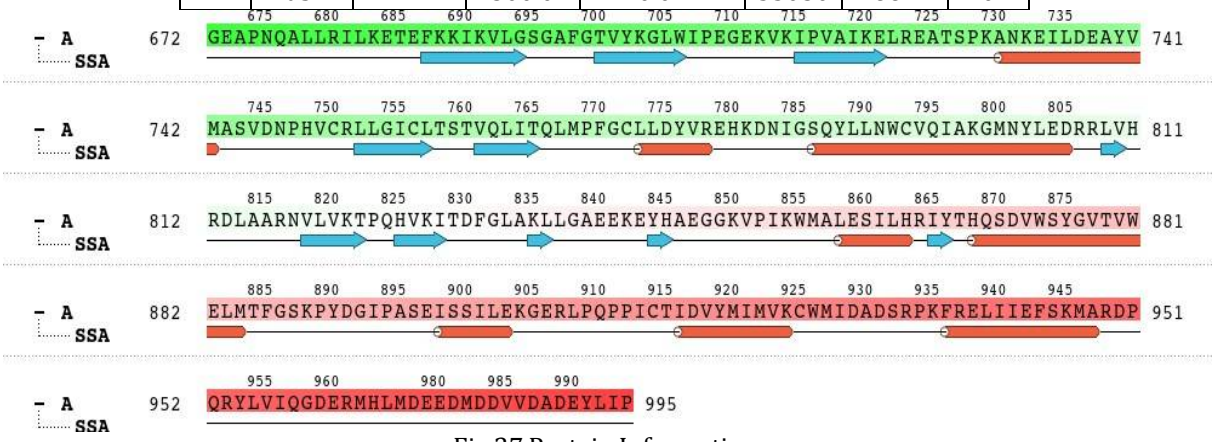

Fig.37.Protein Information

Protein Information

Tot. Residues	Prot. Chain(s)	Res. in Chain(s)	# Atoms	# Heavy Atoms	Charge
312	'A'	312	5032	2497	-6

Ligand Information:

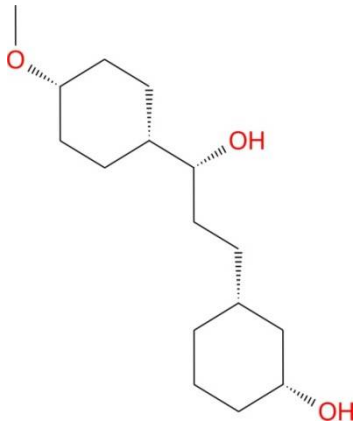

SMILES CO[C@@H](CC1)CC[C@@H]1[C@H](O)CC[C@@H]2C[C@H](O)CCC2 PDB

Name	'LG6'
Num. of Atoms	49 (total) 19 (heavy)
Atomic Mass	270.416 au
Charge	0
Mol. Formula	C16H30O3 Num. of Fragments 1
Num. of Rot. Bonds	7

Table 7: Counter Ion / Salt Information

Counter Ion / Salt Information

Type	Number	Concentration (mM)	Total Charge
Na	52	56.897	+52
Cl	46	50.332	-46

Protein-Ligand RMSD

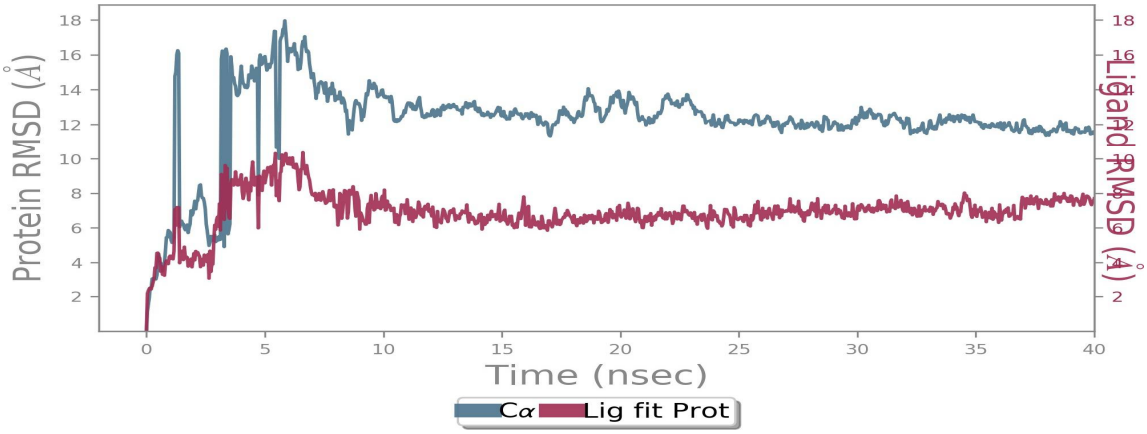

Fig.38 Protein-Ligand RMSD (Root Mean Square Deviation)

The Root Mean Square Deviation (RMSD) is used to measure the average change in displacement of a selection of atoms for a particular frame with respect to a reference frame. It is calculated for all frames in the trajectory. The RMSD for frame *x* is:

$$RMSD_x = \sqrt{\frac{1}{N}\sum_{i=1}^{N}(r_i'(t_x)) - r_i(t_{ref}))^2}$$

Where*N* is the number of atoms in the atom selection; t_{ref} is the reference time, (typically the first frame is used as the reference and it is regarded as time *t*=0); and *r′* is the position of the selected atoms in frame *x* after superimposing on the reference frame, where frame *x* is recorded at time t_x. The procedure is repeated for every frame in the simulation trajectory.

Protein RMSD

The above plot shows the RMSD evolution of a protein (left *Y*-axis). All protein frames are first aligned on the reference frame backbone, and then the RMSD is calculated based on the atom selection.

Monitoring the RMSD of the protein can give insights into its structural conformation throughout the simulation. RMSD analysis can indicate if the simulation has equilibrated — its fluctuations towards the end of the simulation are around some thermal average structure. Changes of the order of 1-3 Å are perfectly acceptable for small, globular proteins. Changes much larger than that, however, indicate that the protein is undergoing a large conformational change during the simulation. It is also important that your simulation converges — the RMSD values stabilize around a fixed value. If the RMSD of the protein is still increasing or decreasing on average at the end of the simulation, then your system has not equilibrated, and your simulation may not be long enough for rigorous analysis.

Ligand RMSD:

Ligand RMSD (right *Y*-axis) indicates how stable the ligand is with respect to the protein and its binding pocket. In the above plot, 'Lig fit Prot' shows the RMSD of a ligand when the protein-ligand complex is first aligned on the protein backbone of the reference and then the RMSD of the ligand heavy atoms is measured. If the values observed are significantly larger than the RMSD of the protein, then it is likely that the ligand has diffused away from its initial binding site.

Protein RMSF

The Root Mean Square Fluctuation (RMSF) is useful for characterizing local changes along the protein chain. The RMSF for residue *i*is:

$$RMSF_i = \sqrt{\frac{1}{T}\sum_{t=1}^{T} < (r_i'(t)) - r_i(t_{ref}))^2 >}$$

Where*T* is the trajectory time over which the RMSF is calculated, t_{ref} is the reference time, $r_i$is the position of residue *i*; *r′* is the position of atoms in residue *i*after superposition on the reference, and the

angle brackets indicate that the average of the square distance is taken over the selection of atoms in the residue.

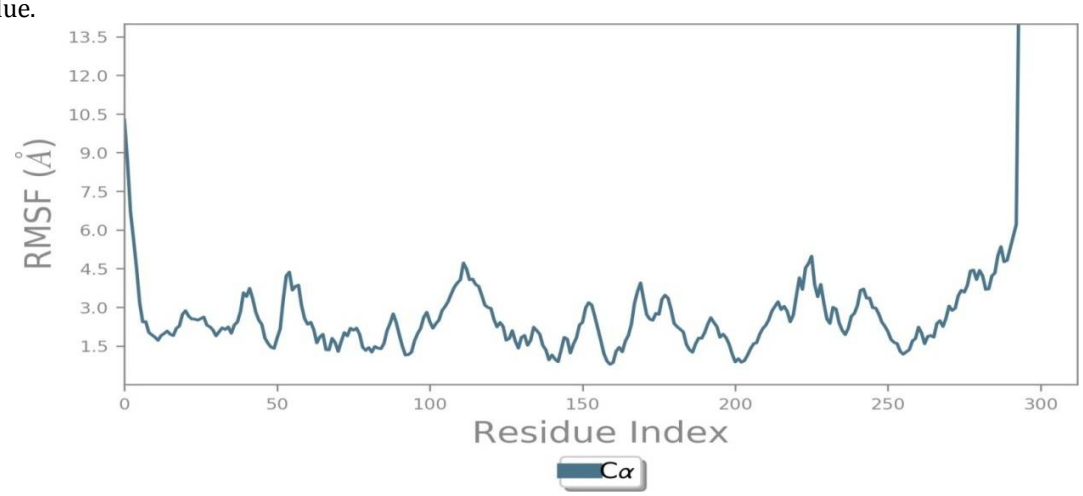

Fig.39 Protein RMSF (Root mean square Fluctuations)

On this plot, peaks indicate areas of the protein that fluctuate the most during the simulation. Typically you will observe that the tails (*N*- and *C*-terminal) fluctuate more than any other part of the protein. Secondary structure elements like alpha helices and beta strands are usually more rigid than the unstructured part of the protein, and thus fluctuate less than the loop regions.

Protein Secondary Structure

% Helix	% Strand	% Total SSE
25.67	16.34	42.01

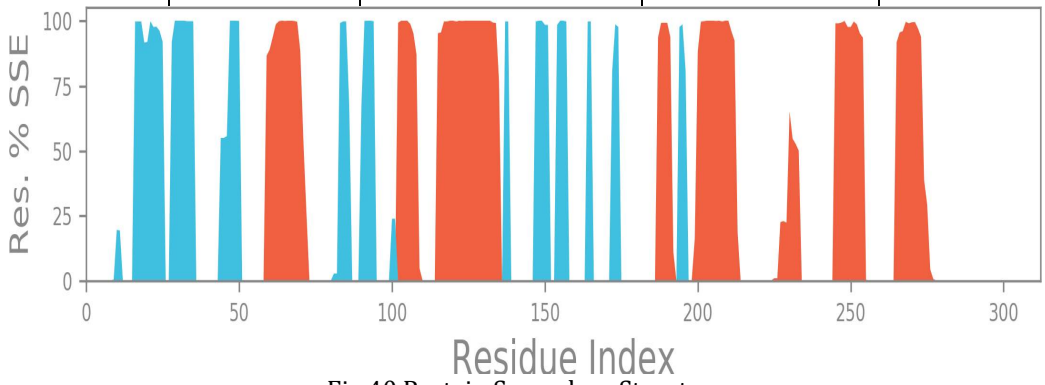

Fig.40 Protein Secondary Structure

Protein secondary structure elements (SSE) like alpha-helices and beta-strands are monitored throughout the simulation. The plot above reports SSE distribution by residue index throughout the protein structure. The plot below summarizes the SSE composition for each trajectory frame over the course of the simulation, and the plot at

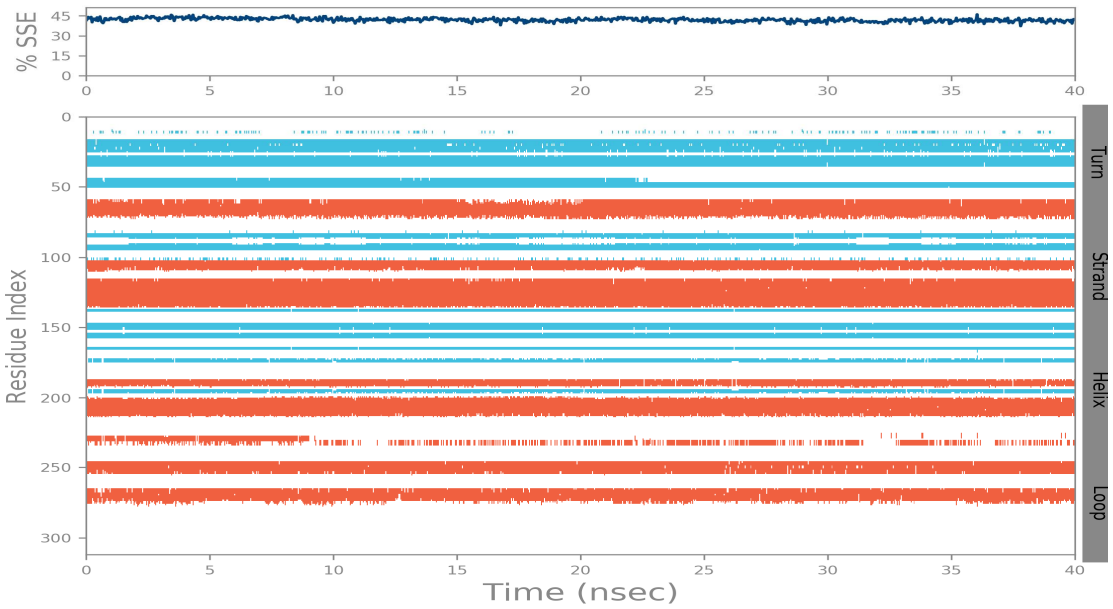

Fig.41. Protein Secondary Structure Elements

The bottom monitors each residue and its SSE assignment over time.

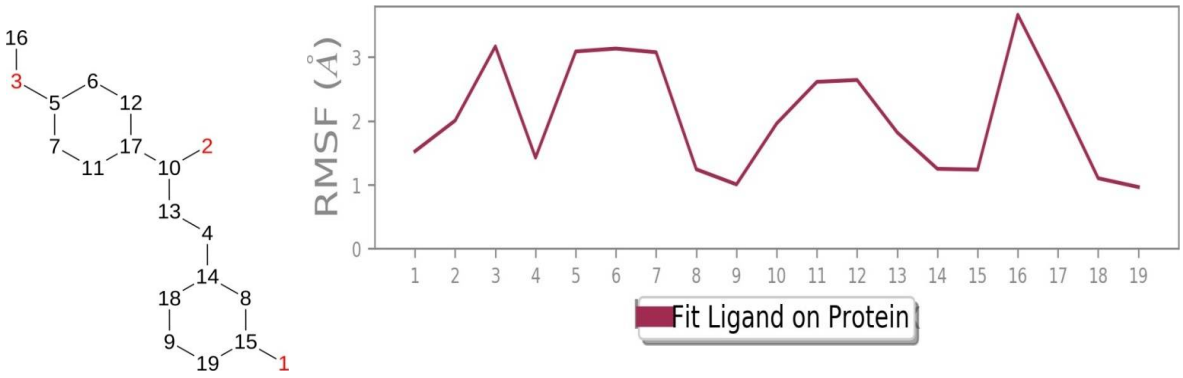

Fig.42. Fit Ligand on Protein

Ligand RMSF:

The Ligand Root Mean Square Fluctuation (L-RMSF) is useful for characterizing changes in the ligand atom positions. The RMSF for atom *i* is:

$$RMSF_i = \sqrt{\frac{1}{T}\sum_{t=1}^{T}(r_i'(t)) - r_i(t_{ref}))^2}$$

Where *T* is the trajectory time over which the RMSF is calculated, t_{ref} is the reference time (usually for the first frame, and is regarded as the *zero* of time); *r* is the position of atom *i* in the reference at time t_{ref}, and *r'* is the position of atom *i* at time *t* after superposition on the reference frame.

Ligand RMSF shows the ligand's fluctuations broken down by atom, corresponding to the 2D structure in the top panel. The ligand RMSF may give you insights on how ligand fragments interact with the protein and their entropic role in the binding event. In the bottom panel, the 'Fit Ligand on Protein' line shows the ligand fluctuations, with respect to the protein. The protein-ligand complex is first aligned on the protein backbone and then the ligand RMSF is measured on the ligand heavy atoms.

Protein-Ligand Contacts

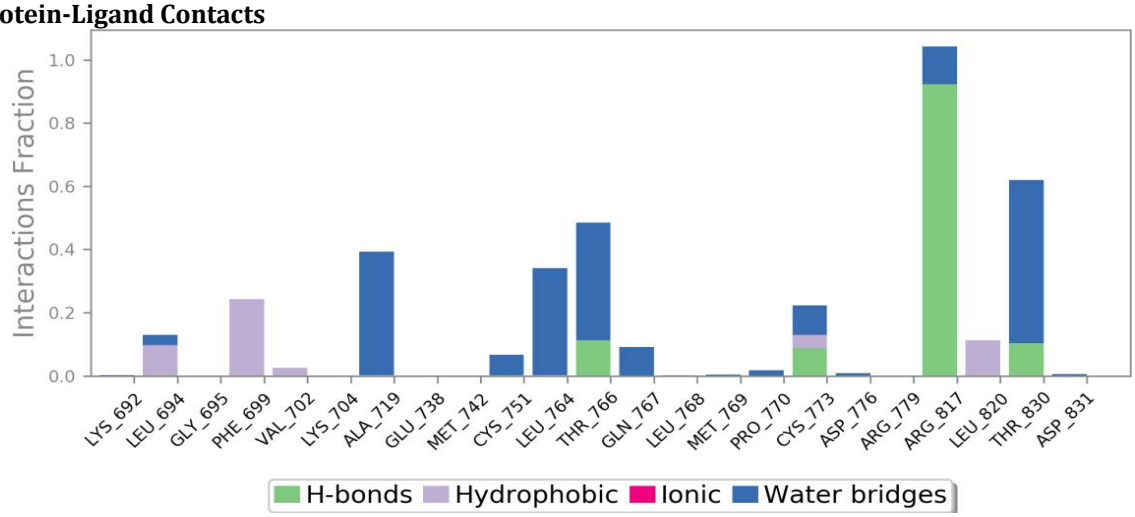

Fig.43 Protein Ligand Contacts

Protein interactions with the ligand can be monitored throughout the simulation. These interactions can be categorized by type and summarized, as shown in the plot above. Protein-ligand interactions (or 'contacts') are categorized into four types: Hydrogen Bonds, Hydrophobic, Ionic and Water Bridges. Each interaction type contains more specific subtypes, which can be explored through the 'Simulation Interactions Diagram' panel. The stacked bar charts are normalized over the course of the trajectory: for example, a value of 0.7 suggests that 70% of the simulation time the specific interaction is maintained. Values over 1.0 are possible as some protein residue may make multiple contacts of same subtype with the ligand.

Hydrogen Bonds:

(H-bonds) play a significant role in ligand binding. Consideration of hydrogen-bonding properties in drug design is important because of their strong influence on drug specificity, metabolization and adsorption. Hydrogen bonds between a protein and a ligand can be further broken down into four subtypes: backbone acceptor; backbone donor; side-chain acceptor; side-chain donor.

The current geometric criteria for protein-ligand H-bond is: distance of 2.5 Å between the donor and acceptor atoms (D—H···A); a donor angle of ≥120° between the donor-hydrogen-acceptor atoms (D—H···A); and an acceptor angle of ≥90° between the hydrogen-acceptor-bonded atom atoms (H···A—X).

Hydrophobic contacts:

fall into three subtypes: π-Cation; π–π; and Other, non-specific interactions. Generally these type of interactions involve a hydrophobic amino acid and an aromatic or aliphatic group on the ligand, but we have extended this category to also include π-Cation interactions.

The current geometric criteria for hydrophobic interactions is as follows: π–Cation — Aromatic and charged groups within 4.5 Å; π–π — Two aromatic groups stacked face-to-face or face-to-edge; Other — A non-specific hydrophobic sidechain within 3.6 Å of a ligand's aromatic or aliphatic carbons.

Ionic interactions: or polar interactions, are between two oppositely charged atoms that are within 3.7 Å of each other and do not involve a hydrogen bond. We also monitor Protein-Metal-Ligand interactions, which are defined by a metal ion coordinated within 3.4 Å of protein's and ligand's heavy atoms (except carbon). All ionic interactions are broken down into two subtypes: those mediated by a protein backbone or side chains.

Water Bridges: are hydrogen-bonded protein-ligand interactions mediated by a water molecule. The hydrogen-bond geometry is slightly relaxed from the standard H-bond definition.

The current geometric criteria for a protein-water or water-ligand H-bond are: a distance of 2.8 Å between the donor and acceptor atoms (D—H···A); a donor angle of ≥110° between the donor-hydrogen-acceptor atoms (D—H···A); and an acceptor angle of ⍰90° between the hydrogen-acceptor-bonded atom atoms (H···A—X).

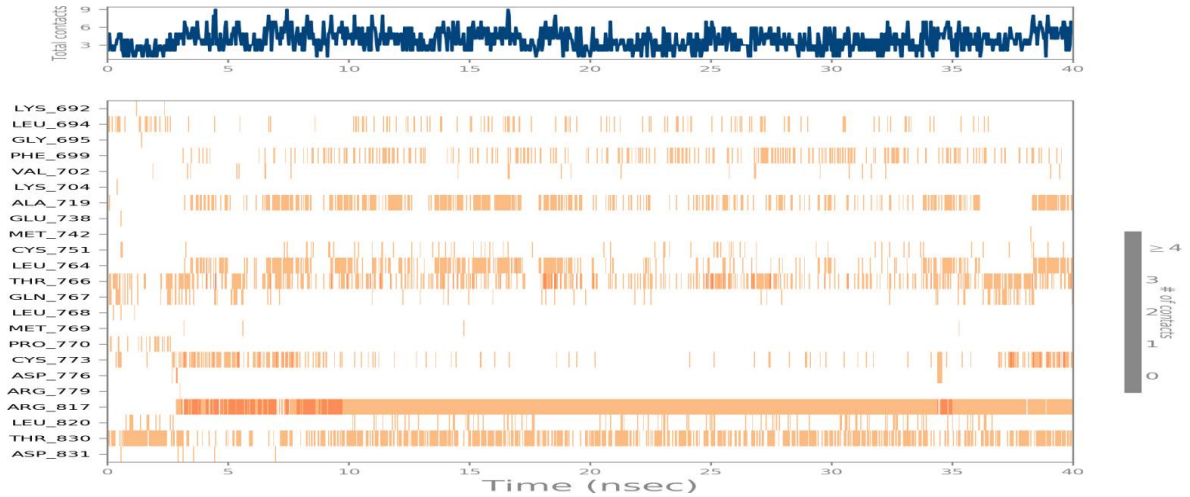

Fig.44 Protein Ligand Contacts

Protein-Ligand Contacts (cont.) A timeline representation of the interactions and contacts (H-bonds, Hydrophobic, Ionic, Water bridges) summarized in the previous page. The top panel shows the total number of specific contacts the protein makes with the ligand over the course of the trajectory. The bottom panel shows which residues interact with the ligand

In each trajectory frame. Some residues make more than one specific contact with the ligand, which is represented by a darker shade of orange, according to the scale to the right of the plot.

Ligand-Protein Contacts:

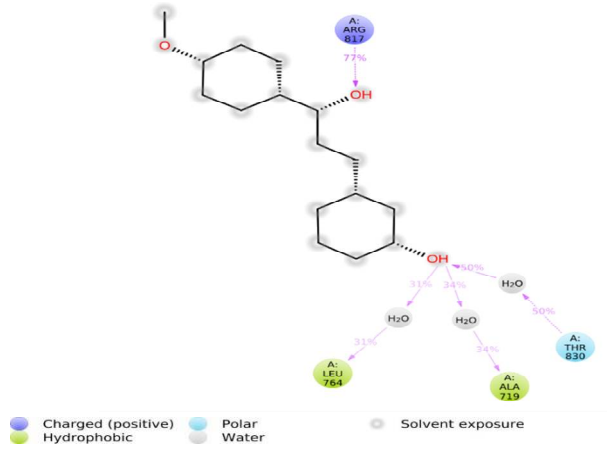

Fig. 45: ligand atom interactions with the protein residues

A schematic of detailed ligand atom interactions with the protein residues. Interactions that occur more than**30.0%** of the simulation time in the selected trajectory (0.00 through 40.00 nsec), are shown.Note: it is possible to have interactions with >100% as some residues may have multiple interactions of a single type with the same ligand atom. For example, the ARG side chain has four H-bond donors that can all hydrogen-bond to a single H-bond acceptor.

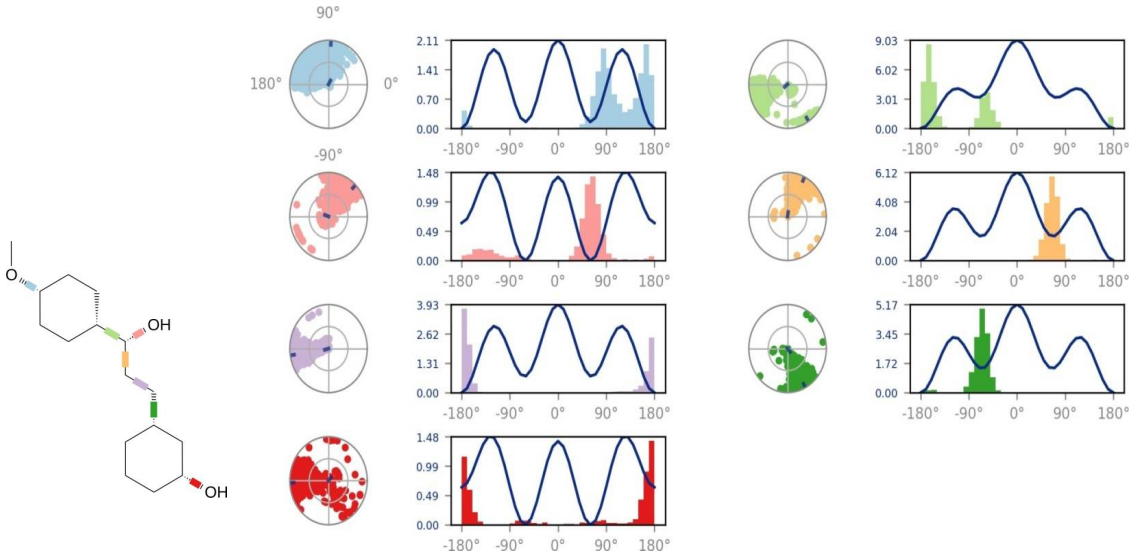

Fig.46: Ligand Torsion Profile

Ligand Torsion Profile

The ligand torsions plot summarizes the conformational evolution of every rotatable bond (RB) in the ligand throughout the simulation trajectory (0.00 through 40.00 nsec). The top panel shows the 2d schematic of a ligand with color-coded rotatable bonds. Each rotatable bond torsion is accompanied by a dial plot and bar plots of the same color.

Dial (or radial) plots describe the conformation of the torsion throughout the course of the simulation. The beginning of the simulation is in the center of the radial plot and the time evolution is plotted radially outwards.

The bar plots summarize the data on the dial plots, by showing the probability density of the torsion. If torsional potential information is available, the plot also shows the potential of the rotatable bond (by summing the potential of the related torsions). The values of the potential are on the left *Y*-axis of the chart, and are expressed in *kcal/mol*. Looking at the histogram and torsion potential relationships may give insights into the conformational strain the ligand undergoes to maintain a protein-bound conformation.

Ligand Properties

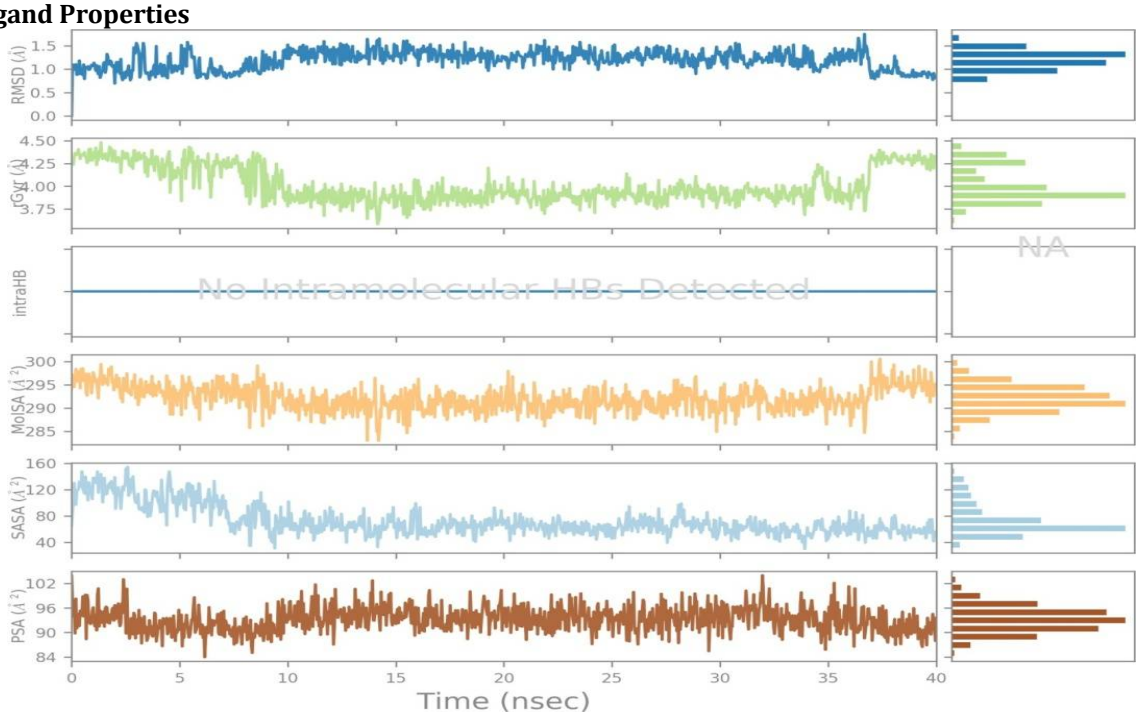

Fig.47 Ligand-Properties

Ligand RMSD: Root mean square deviation of a ligand with respect to the reference conformation (typically the first frame is used as the reference and it is regarded as time *t*=0).

Radius of Gyration (rGyr): Measures the 'extendedness' of a ligand, and is equivalent to its principal moment of inertia.
Intramolecular Hydrogen Bonds (intraHB): Number of internal hydrogen bonds (HB) within a ligand molecule.
Molecular Surface Area (MolSA): Molecular surface calculation with 1.4 Å probe radius. This value is equivalent to a van der Waals surface area.
Solvent Accessible Surface Area (SASA): Surface area of a molecule accessible by a water molecule.
Polar Surface Area (PSA): Solvent accessible surface area in a molecule contributed only by oxygen and nitrogen atoms.

DISCUSSION

In the case of EGFR enzyme, the binding energy of each selected ligands (LG1-LG8) has been found to be higher than that of reference molecule LG0. The binding of all the compounds ranges from (-7.5 to -8 kJ/mol) where the binding energy of reference molecule LG0 is -7.4. The interaction profile shown that the reference molecule mainly interact with THR766, CYS773, ASP831 and THR830 whereas the other ligands also have shown interactions with other residues GLU738, MET769, LEU764, ALA719 and LYS721. The ligand LG6 has the lowest binding energy i.e. -8 kJ/mol among all eight compounds. It interacts with residues THR766, LEU764, ALA719, LYS721, MET769 of EGFR enzyme. Compounds LG6 and LG1 also have several non-bonded interactions presents.
For NOS enzyme, the binding energy of reference molecule i.e. LG0 is -6.5 kJ/mol. The other selected compounds for docking have binding energy greater than reference compound except LG1 and LG3. Compounds LG1 and LG3 has binding energy -6.4 kJ/mol. The binding energy of remaining compounds ranges from (-6.6 to -7.2 kJ/mol). The compound LG2 and LG4 have lowest binding energy among all docked compounds. The reference molecule has shown to interact with GLU377, ASP382, TYR373, GLN263, ALA262, TYR347, ARG266 residues of NOS enzyme. The compounds selected for docking i.e. (LG1-LG8) also interact with other residues VAL352, ASP385, ARG381, ALA282, ASN354, ARG388. Also compounds LG6 and LG7 interact with cofactor H4B of NOS enzyme. LG4 also have shown higher residue interaction than LG2.

ACKNOWLEDGMENT

The authors would like to place thanks to Mr. Biologist team (http://www.askmrbiologist.com/) 506, wing A, Anantshilp Society Bavdhan, Pin: 41102Pune, Maharashtra for providing required facilities to carry out this research work.

REFERENCES

1. Huang, S.Y. &Zou, X.(2010).Advances and Challenges in Protein-Ligand Docking. Int. J. Mol. Sci., 11(8): 3016-3034.
2. Sousa, S.F., Fernandes, P.A. & Ramos, M.J. (2006).Protein-ligand docking: Current status and future challenges. Proteins Structure Function. Bioinf., 65(1):15-26.
3. Novikov, F.N. &Chilov, G.G., (2009).Molecular docking: theoretical background, practical applications and perspectives. Mendeleev Commun., 19(5):237-242.
4. Balaji, G.A., Balaji, V. N. & Rao, S.N., (2013).Utility of scoring function customization in docking-based virtual screening approaches. Current Sci., 104(1):86-97.
5. Berman, H.M., Westbrook, J., Feng, Z., Gilliland, G., Bhat, T. N., Weissig, H., Shindyalov, I.N. & Bourne, P.E. (2000).The Protein Data Bank. Nucleic Acids Research., 28:235-242.
6. Bernstein, F.C., Koetzle, T.F., Williams, G.J.B., Meyer, E.F. Jr., Brice, M.D., Rodgers, J.R., Kennard, O., Shimanouchi, T. &Tasumi, M. (1978).The protein data bank: A computer-based archival file for macromolecular structures. Arch. Biochem. Biophys., 185(2):584-591.
7. Elshemy, H.A.H. &Zaki, M.A. (2017).Design and synthesis of new coumarin hybrids and insight into their mode of antiproliferative action. Bioorg. Med. Chem., 25:1066-1075.
8. Bray, F., Ferlay, J., Soerjomataram, I., Siegel, R.L., Torre, L.A. &Jemal, A. (2018).Global cancer statistics 2018: GLOBOCAN estimates of incidence and mortality worldwide for 36 cancers in 185 countries. CA Cancer J. Clin., 68:394-424.
9. Hao, Y., Lyu, J., Qu, R., Tong, Y., Sun, D., Feng, F., Tong, L., Yang, T., Zhao, Z., Zhu, L., Ding, J., Xu, Y., Xie, H. & Li, H. (2018).Design, Synthesis and biological evaluation of pyrimido [4,5- d] pyrimidine-2,4(1 h, 3 h) - diones as potent and selective epidermal growth factor receptor (EGFR) inhibitors against L858R/T790M resistance mutation. J. Med. Chem., 61(13):5609-5622.
10. Bonomi, P. (2003). Erlotinib: a new therapeutic approach for non-small cell lung cancer. Expert Opin. Inv. Drug., 12(8):1395-1401.

11. Kobayashi, S., Boggon, T. J., Dayaram, T., Jänne, P. A., Kocher, O., Meyerson, M., Johnson, B. E., Eck, M.J., Tenen, D. G. &Halmos, B. (2005).EGFR mutation and resistance of non-small-cell lung cancer to Gefitinib. New Engl. J. Med., 352(8):786-792.
12. Ou, S.H.I. (2012).Second-generation irreversible epidermal growth factor receptor (EGFR) tyrosine kinase inhibitors (TKIs): a better mousetrap? A review of the clinical evidence. Crit. Rev. Oncol. Hemat., 83(3):407-421.
13. 13.Gaber, A.A., Bayoumi, A.H., El-morsy, A.M., Sherbiny, F.F., Mehany, A.B.M. &Eissa, I.H. (2018).Design, synthesis and anticancer evaluation of 1H-pyrazolo[3,4-*d*]pyrimidine derivatives as potent EGFRWT and EGFRT790M inhibitors and apoptosis inducers. Bioorg. Chem., 80:375-395.
14. 14.Walter, A.O., Sjin, R.T.T., Haringsma, H.J., Ohashi, K., Sun, J., Lee, K., Dubrovskiy, A., Labenski, M., Zhu, Z., Wang, Z., Sheets, M., Martin, T.S., Karp, R., Kalken, D.V., Chatuverdi, P., Niu, D., Nacht, M., Petter, R.C., Westlin, W., Lin, K., Jaw-Tsai, S., Raponi, M., Dyke, T.V., Etter, J., Weaver, Z., Pao, W., Singh, J., Simmons, A.D., Harding, T.C. & Allen, A. (2013).Discovery of a mutant-selective covalent inhibitor of EGFR that overcomes T790M mediated resistance in NSCLC. Cancer Discov., 3(12):1404-1415.
15. 15.Chen, L., Fu, W., Zheng, L., Liu, Z. & Liang, G. (2018).Recent progress of small-molecule epidermal growth factor receptor (EGFR) inhibitors against C797S resistance in non-small-cell lung cancer. J. Med. Chem., 61(10):4290-4300.
16. 16.Yver, A. (2016).Osimertinib (AZD9291) a science-driven, collaborative approach to rapid drug design and development. Ann. Oncol., 27(6):1165-1170.
17. 17. Lin, S., Li, Y., Zheng, Y., Luo, L., Sun, Q., Ge, Z., Cheng, T. & Li, R. (2017).Design, synthesis and biological evaluation of quinazoline-phosphoramidate mustard conjugates as anticancer drugs. Eur. J. Med. Chem., 127:442-458.
18. 18. Cramer, R.D., Patterson, D.E. &Bunce, J.D. (1988). Comparative molecular field analysis (CoMFA): Effect of shape on binding of steroids to carrier proteins. J. Am. Chem. Soc., 110(18):5959-5967.
19. 19.Klebe, G., Abraham, U. &Mietzner, T. (1994).Molecular similarity indices in a comparative analysis (CoMSIA) of drug molecules to correlate and predict their biological activity. J. Med. Chem., 37(24):4130-4146.
20. 20. Ferlay, J., Soerjomataram, I., Dikshit, R., Eser, S., Mathers, C., Rebelo, M., Parkin, D.M., Forman, D. & Bray, F. (2015).Cancer incidence and mortality worldwide: sources, methods and major patterns in GLOBOCAN 2012. Inter. J. Cancer. 136: E359-E386.
21. 21. Marder, M., Viola, H., Bacigaluppo, J. A., Colombo, M. I., Wasowski, C., Wolfman, C. &Paladini, A. C. (1998).Detection of benzodiazepine receptor ligands in small libraries of flavone derivatives synthesized by solution phase combinatorial chemistry. Biochem. biophy. Res. Comm., 249:481-485.
22. 22. Nagaoka, T., Banskota, A. H., Tezuka, Y., Saiki, I. &Kadota, S. (2002). Selective antiproliferative activity of caffeic acid phenethyl ester analogues on highly liver-metastatic murine colon 26-L5 carcinoma cell line. Bioorg. Med. Chem., 10:3351-3359.
23. 23. Alonso, D. F., Farías, E. F., Urtreger, A., Ladeda, V., Vidal, M. D. C. C. &Bal, De Kier Joffe, E. (1996). Characterization of F3II, a sarcomatoid mammary carcinoma cell line originated from a clonal subpopulation of a mouse adenocarcinoma. J. Sr. Oncol., 62:288-297.
24. 24. Takagaki, N., Sowa, Y., Oki, T., Nakanishi, R., Yogosawa, S. & Sakai, T. (2005). Apigenin induces cell cycle arrest and p21/WAF1 expression in a p53-independent pathway. Inter. J. Oncol., 26:185-190.
25. 25.Tripathi, P.; Tripathi, P., Kashyap, L. & Singh, V. (2007). The role of nitric oxide in inflammatory reactions. FEMS Immunol. Med. Microbiol., 51:443-452.
26. 26.Cheng, J. H., Hung, C. F., Yang, S. C., Wang, J. P., Won, S. J. & Lin, C. N. (2008). Synthesis and cytotoxic, anti-inflammatory, and anti-oxidant activities of 2',5'-dialkoxylchalcones as cancer chemopreventive agents. Bioorg. Med. Chem., 16:7270-7276.
27. 27. Ko, H. H., Tsao, L. T., Yu, K. L., Liu, C. T., Wang, J. P. & Lin, C. N. (2003). Structure-activity relationship studies on chalcone derivatives. The potent inhibition of chemical mediator's release.Bioorg. Med. Chem., 11:105-111.
28. Bogdan, C., Rollinghoff, M. &Diefenbach, A. (2000). The role of nitric oxide in innate immunity. Immunol. Rev., 173:17-26.
29. Moncada, S., Palmer, R.M. & Higgs, E.A. (1991).Nitric oxide: physiology, pathophysiology and pharmacology. Pharmacol. Rev., 43:109-142.
30. Nakagawa, T. &Yokozawa, T. (2002).Direct scavenging of nitric oxide by green tea. Food Chem. Toxicol., 40:1745-1750.
31. Taira, J., Nanbu, H. & Ueda, K. (2009).Nitric oxide-scavenging compounds in *Agrimoniapilosa* Ledeb on LPS-induced RAW264.7 macrophages. Food Chem., 115:1221-1227.
32. Pacher, P., Beckman, J. S. &Liaudet, L. (2007).Nitric oxide and peroxynitrite in health and disease. Physiol. Rev., 87:315-424.
33. Lenon, G.B., Li, C.G., Xue, C.C., Thien, F.C.K. & Story, D.F. (2008).Inhibition of inducible nitric oxide production and iNOS protein expression in lipopolysaccharide-stimulated rat aorta and Raw 264.7 macrophages by ethanol extract of a Chinese herbal medicine formula (RCM-101) for allergic rhinitis. J. Ethnopharmacol., 116:547-553.
34. Moncada, S., Palmer, R.M. & Higgs, E.A. (1991). Nitric oxide: physiology, pathophysiology, and pharmacology. Pharmacol. Rev., 43:109-142.
35. Nicholas, C., Batra, S., Vargo, M.A., Voss, O.H., Gavrilin, M.A., Wewers, M.D., Guttridge, D. C., Grotewold, E. &Doseff, A.I. (2007).Apigenin blocks lipopolysaccharide-induced lethality in *vivo* and proinflammatory cytokines

expression by inactivating NF-kappaB through the suppression of p65 phosphorylation. J. Immunol., 179:7121-7127.
36. http://autodock.scripps.edu/
37. Schrödinger Release 2017-1:QikProp, Schrödinger, LLC, New York, NY, 2017. Schrodinger Inc. Report generated 12-23-2019 15:50